JEM Journal of Experimental Medicine

ARTICLE

AMFR drives allergic asthma development by promoting alveolar macrophage–derived GM-CSF production

Huihui Zhang[1], Ran Wei[2], Xinyi Yang[1], Lu Xu[1], Hongchao Jiang[1], Mengkai Li[1], Haixia Jiang[3], Haibo Zhang[1], Zhihong Chen[4], Feng Qian[1]*, and Lei Sun[1]*

Alveolar macrophages (AMs) are specialized tissue-resident macrophages that orchestrate the immune response in allergic inflammation and asthma. However, what signals direct AMs to cross talk with other immune cells remains unclear. Here, we report that autocrine motility factor receptor (AMFR), an endoplasmic reticulum–resident E3 ubiquitin ligase, is upregulated in AMs of asthma and is critical for this condition. AMFR deficiency significantly decreased allergy-induced T helper 2 (Th2) and eosinophilic inflammation, with less granulocyte-macrophage colony-stimulating factor (GM-CSF) production in AMs. Mechanistically, following thymic stromal lymphopoietin (TSLP) stimulation, AMFR associated directly with cytokine-inducible SH2-containing protein (CIS), induced the ubiquitination of Lys48-linked polyubiquitination of CIS, and consequently blocked the inhibitory effect of CIS on signal transducer and activator of transcription 5 (STAT5) phosphorylation and the downstream pathway activation in AMs. In conclusion, our results demonstrate that AMFR serves a crucial role in promoting inflammation in asthma through regulating AM function, and may emerge as a new potential drug target for asthma therapy.

Introduction

Asthma represents a global health issue and economic burden, with >300 million people currently affected by it, a number that will increase by another 100 million during the next decades (Adhikary et al., 2021; Stern et al., 2020). This condition, which stems from a complex interrelationship of genetic, immunologic, environmental, and pharmacological factors, is characterized by airway hyperresponsiveness and chronic inflammation (Lin et al., 2017). Despite an increasing exploration of the genetics and epigenetics of asthma, its underlying immune mechanisms remain unclear, leading to unsatisfactory diagnosis and treatment (Moore et al., 2013). Therefore, achieving a better understanding of the immune mechanisms involved in airway inflammation is critical for improving the treatment of asthma.

Alveolar macrophages (AMs), a prominent immune cell type in the airways, play an essential role in homeostasis, tissue remodeling, and host defense in the lung (Evren et al., 2020; Joshi et al., 2018). Recently, accumulating studies have revealed that AMs contribute to the development and progression of asthma. These cells mediate the allergic antigen presentation in asthma, facilitating the recruitment of activated neutrophils to the alveolar space, and efficiently clearing cellular debris (Fehervari, 2015; Puttur et al., 2019). Additionally, researchers have emphasized the immunoregulatory functions of AMs, given that they modulate T helper 2 (Th2) and eosinophilic inflammation in asthma. By producing various cytokines, such as GM-CSF, IL-1β, IL-6, IL-8, and TGF-β, AMs can directly stimulate the proliferation and differentiation of Th2 cells (Lambrecht et al., 2019). Furthermore, cytokines produced by AMs, such as chemokine (C-C motif) ligand 3 (CCL3), CCL5, CCL17, CCL22, CCL24, and GM-CSF, can also mediate the recruitment, retention, degranulation, and cytokine production of eosinophils within inflamed sites, thus worsening disease complications (Evren et al., 2020; Kulikauskaite and Wack, 2020). Based on the functional diversity of AMs, they are widely regarded as an effective therapeutic target in asthma (Song et al., 2018). However, the detailed mechanisms by which AMs regulate cell–cell cross talk in the inflammatory microenvironment in asthma need to be elucidated.

[1]Engineering Research Center of Cell & Therapeutic Antibody, Ministry of Education, Pharm-X Center, School of Pharmacy, Shanghai Jiao Tong University, Shanghai, P.R. China; [2]State Key Laboratory of Oncology in South China, Collaborative Innovation Center for Cancer Medicine, Sun Yat-sen University Cancer Center, Guangzhou, P.R. China; [3]School of Life Sciences & Biotechnology, Shanghai Jiao Tong University, Shanghai, P.R. China; [4]Department of Respiratory and Critical Care Medicine of Zhongshan Hospital, Shanghai Institute of Respiratory Disease, Fudan University, Shanghai, P.R. China.

*L. Sun and F. Qian contributed equally to this paper. Correspondence to Lei Sun: sunlei_vicky@sjtu.edu.cn; Feng Qian: fengqian@sjtu.edu.cn.

Recently, the ubiquitin protein degradation system (UPS) has emerged as a central element in the pathogenesis and development of asthma (Popovic et al., 2014; Sahoo, 2014). It has been reported that E3 ubiquitin (Ub) ligases, including Grail, Itch, and Cbl-b, control T cell activation, resulting in the suppression of allergic airway inflammation (Liu, 2007; Qiao et al., 2014; Sahoo et al., 2014). In addition, E3 Ub ligase March1 was found to regulate the development of allergic inflammatory response by promoting Th2 cytokines (Kishta et al., 2018). Moreover, E3 Ub ligase Midline 1 was demonstrated to promote allergen and rhinovirus-induced asthma by inhibiting protein phosphatase 2A activity in mouse bronchial epithelium (Collison et al., 2013). Therefore, ubiquitination and degradation of critical signaling molecules seem to play a crucial role in maintaining immune tolerance in different effector arms of the T cell and epithelium system. However, how the Ub proteasome system regulates AM function in asthma is not yet fully understood.

To address these questions, we performed RNA sequencing (RNA-seq) analysis of purified AMs from two murine models of asthma, from which we identified that E3 Ub ligase autocrine motility factor receptor (AMFR) was upregulated in both OVA- and papain-induced asthma in mice. AMFR, also known as gp78, is an ER-resident E3 Ub ligase that recognizes misfolded proteins for ubiquitylation and subsequent degradation by the proteasome in an ER-associated degradation (ERAD) manner (Joshi et al., 2017). Numerous studies have described the crucial role of AMFR in cellular signaling (Luo et al., 2002), tumor formation and metastasis (Fu et al., 2013), neurodegenerative diseases (Ying et al., 2011), and innate immune response (Wang et al., 2014), among others. In the present study, we generated a myeloid-specific AMFR deficiency mouse model to demonstrate its role in the pathogenesis of asthma, gaining evidence that AMFR controls thymic stromal lymphopoietin (TSLP)–stimulated cytokine-inducible SH2-containing protein (CIS) degradation, thus initiating GM-CSF production and driving allergic asthma. Our study highlights novel mechanistic insights into the communication between AMs and Th2 cells and eosinophils, making AMFR an attractive pharmacological target for the development of selective inhibitors for asthma treatment.

Results

AMFR is upregulated in asthmatic AMs

To better identify the functional pathways and important candidate genes contributing to the role of AMs in asthma, we performed a comparative transcriptome analysis using RNA-seq between AMs from asthmatic mice (induced with OVA or papain) and PBS mice (Fig. 1, A and B; and Fig. S1 A). From this analysis, we identified 626 differentially expressed genes (DEGs) in the OVA vs. PBS group (Table S1). Among these, 276 DEGs were upregulated, and 350 DEGs were downregulated. In the papain-induced model, of 295 DEGs that were found, 73 were upregulated, and 222 were downregulated (Table S2). The distribution trends of DEGs in the pairwise comparisons are presented as volcano plots in Fig. 1, C and D.

To further investigate the DEGs involved in regulating AM function in asthmatic inflammation, we conducted a Kyoto Encyclopedia of Genes and Genomes (KEGG) pathway analysis. As shown in Fig. 1, E and F, signal transduction and immune system categories that were most related to asthma, including "Th1/Th2 cell differentiation," "cytokine-cytokine receptor interaction," and "JAK-STAT signaling pathway," had an advantage in gene enrichment. In addition, a few Ub-related pathways were significantly enriched in both the OVA vs. PBS group, and papain vs. PBS group, including "protein processing in endoplasmic reticulum" and "ubiquitin mediated proteolysis." Moreover, the Gene Ontology (GO) analysis of these DEGs identified several significant pathways that presented patterns similar to those from the KEGG analysis, such as biological processes related to "response to cytokine," "cell surface receptor signaling pathway," "cytokine-mediated signaling pathway," and molecular functions related to "ubiquitin-ubiquitin ligase activity" and "cytokine activity" (Fig. S1, B and C). Thus, these results suggest that the DEGs of the Ub-mediated proteolysis may be critical to regulating AMs in asthma. To further explore the role of Ub-mediated proteolysis in asthma, we analyzed 205 E3 Ub ligases genes in the GO database with the DEGs (Table S3). According to our results, a few Ub-related genes were found with DEGs in either the OVA group or the papain group; however, only *Amfr* was found to be a DEG of both groups (Fig. 1 G). In addition, the Western blot assay (Fig. 1 H) and immunohistochemical staining (Fig. 1 I) further confirmed the upregulation of AMFR expression in AMs of OVA-induced asthmatic mice. Interestingly, immunohistochemical staining showed that nearly all cells positive for AMFR were circular or elliptic and were characterized by short membrane protrusions (Fig. 1 I). By fluorescent microscope, we observed that a considerable proportion of intracellular AMFR colocalized with CD68 (macrophage marker)-positive AMs in the lung tissues of OVA-induced asthmatic mice (Fig. 1 J). We also assessed the expression of AMFR in other lung myeloid cells, including interstitial macrophages (IMs), pulmonary monocytes, eosinophils, neutrophils, and dendritic cells (DCs; Fig. S1 D). We found that although the expression of AMFR was also upregulated in IMs and monocytes of OVA-induced asthmatic mice, the relative level was lower in comparison with AMs. In addition, despite eosinophils, neutrophils, and DCs expressing lower levels of AMFR, expression did not change significantly in OVA-induced mice compared with PBS mice (Fig. 1 K). Taken together, these data demonstrate that AMFR is almost exclusively upregulated in AMs in asthma.

AMFR promotes eosinophil accumulation and Th2 reaction in allergic asthma induced by OVA or papain

To explore the potential pathophysiological role of AMFR in AMs in asthma, we generated myeloid-specific AMFR-deficient mice (referred to as LysM^{Cre}*Amfr*$^{fl/fl}$) by breeding *Amfr*-floxed mice (*Amfr*$^{fl/fl}$) with Lysozyme M-Cre mice (LysM^{Cre}; Fig. S2 A). We detected WT and recombined alleles by PCR analysis (Table S4 and Fig. S2 B). Additionally, Western blot analysis showed that AMFR protein expression in LysM^{Cre}*Amfr*$^{fl/fl}$ mice was completely deleted in bone marrow–derived macrophages (BMDMs), whereas it remained unchanged in lung tissues (Fig. S2, C and D). Then, we treated *Amfr*$^{fl/fl}$ and LysM^{Cre}*Amfr*$^{fl/fl}$ mice with OVA to induce the allergic asthma model following the standard

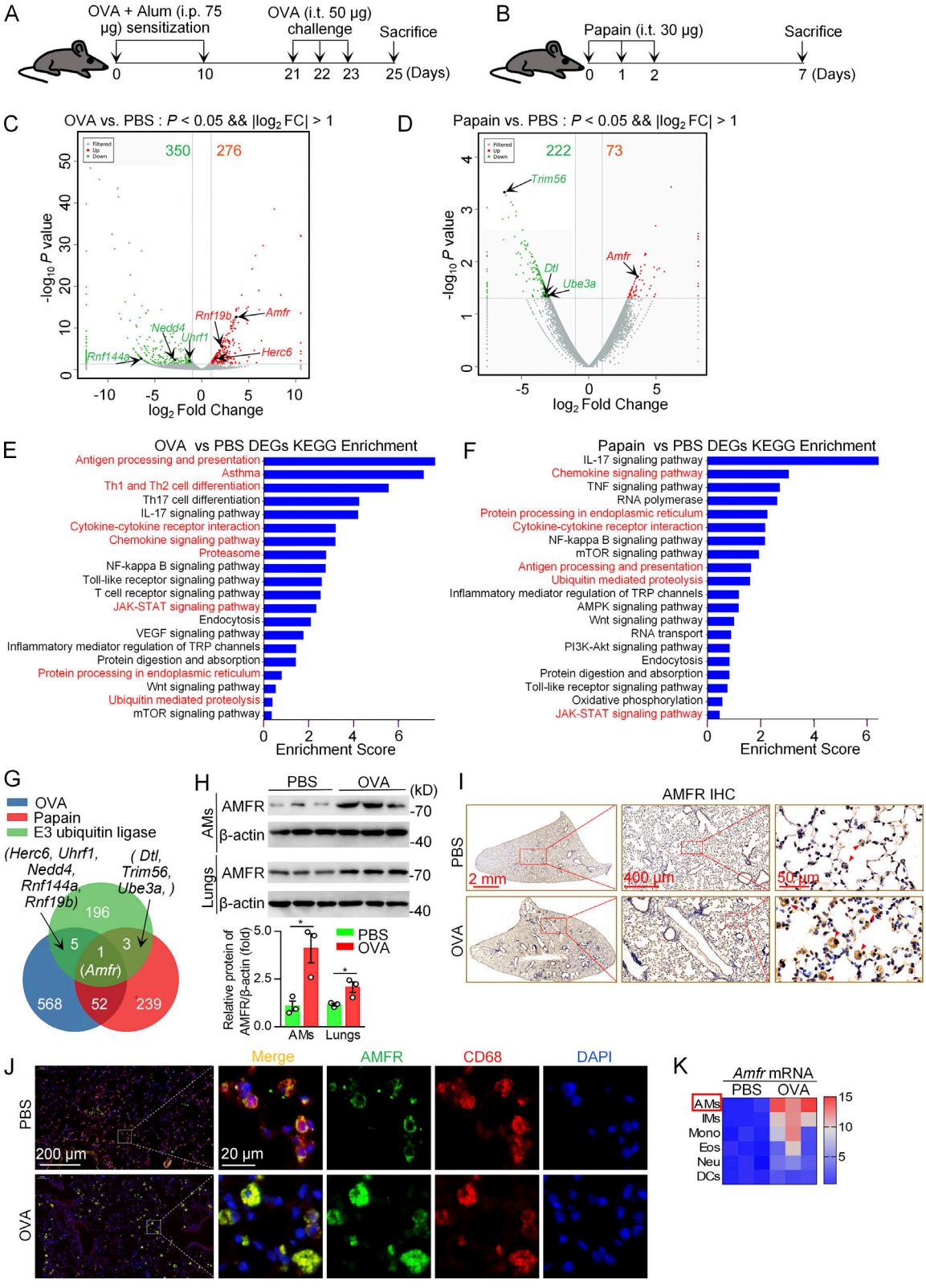

Figure 1. **AMFR is upregulated in asthmatic AMs. (A)** Schematic protocol of the OVA-induced asthma model. Mice were sensitized with 75 μg OVA + Alum adjuvant i.p. on days 0 and 10, and then challenged with OVA (50 μg) i.t. on days 21, 22, and 23. On day 25, asthma was detected. **(B)** Schematic graph of the papain-induced asthma model. Mice were sensitized with 30 μg papain (i.t.) on days 0, 1 and 3, and then sacrificed on day 7. **(C and D)** Volcano plots for DEGs screened by RNA-seq in AMs of mice with OVA- or papain-induced asthma compared with PBS mice. DEGs were defined using the following criteria: FC, fold-change <0.5 or >2 and P < 0.05. **(E and F)** KEGG enrichment analysis of DEGs in the OVA vs. PBS group and papain vs. PBS group, respectively. **(G)** Venn diagram of the overlap from 205 E3 Ub ligases genes in the GO database, and DEGs in the OVA and papain groups. **(H)** Immunoblot analysis of AMFR protein

expression in lung tissues and AMs from WT mice challenged with OVA. The lower panel shows the quantification of the immunoblots in the upper panel, presented as the ratio of AMFR to β-actin. Each symbol represents one mouse. Data are presented as mean ± SD from one representative of three independent experiments. *, P < 0.05 (Student's *t* test). **(I)** Immunohistochemical (IHC) examination of AMFR expression in lung tissues of OVA-induced mice. Scale bars: 2 mm, 400 µm, and 50 µm. **(J)** Immunofluorescence analysis of AMFR expression in the lung tissues. AMFR (green), AM marker CD68 (red), cell nucleus (DAPI, blue), merge (AMFR + CIS + DAPI); scale bars: 200 and 20 µm. **(K)** Heatmap summarizing *Amfr* mRNA expression in lung AM, IMs, eosinophils (Eos), monocytes (Mono), neutrophils (Neu), and DCs from PBS and OVA mice. Data shown are representative of three independent experiments (H–J). Source data are available for this figure: SourceData F1.

protocol (Fig. 1 A). Our data showed that the parameter, response of microvascular permeability, was reduced in the OVA-induced LysM^{Cre}*Amfr*$^{fl/fl}$ mice compared with those in *Amfr*$^{fl/fl}$ mice, including total cell number (Fig. 2 A) and protein concentration (Fig. 2 B) in bronchoalveolar lavage fluid (BALF). In addition, we evaluated the pathological changes in lung tissues after stimulation with OVA using H&E and periodic acid–Schiff (PAS) staining. As shown in Fig. 2 E, OVA induced evident narrowing of the airways with severe infiltration of inflammatory cells in peribronchiolar lung, goblet cell hyperplasia, and production of mucus in *Amfr*$^{fl/fl}$ mice. However, these responses were ameliorated in LysM^{Cre}*Amfr*$^{fl/fl}$ mice. Collectively, these results demonstrate that AMFR is necessary for OVA-induced allergic asthma.

Next, we used papain (a proteolytic enzyme used in food industries and related to occupational asthma) to induce asthma (Kabata et al., 2015), and evaluated the role of AMFR in this model of asthmatic pathogenesis according to the standard protocol (Fig. 1 B). Similar to the results observed in the OVA-induced asthma model, total cell number (Fig. 2 C) and protein concentration (Fig. 2 D) in BALF from LysM^{Cre}*Amfr*$^{fl/fl}$ mice were lower than those from *Amfr*$^{fl/fl}$ mice after papain stimulation. Consistently, the pathological staining with H&E and PAS also showed inhibition of goblet cell hyperplasia, along with decreased cell infiltration and mucus production in the bronchial epithelium in LysM^{Cre}*Amfr*$^{fl/fl}$ mice, compared with those in *Amfr*$^{fl/fl}$ mice (Fig. 2 F). Based on these results, AMFR is also critical for papain-induced allergic asthma.

Besides airway hyperresponsiveness, allergic asthma is characterized by an allergen-triggered eosinophilic infiltration, a strong Th2 immune response associated with enhanced production of IL-4, IL-5, and IL-13, and the presence of IgE (Holgate, 2012). The flow cytometry assay showed that AMFR deficiency led to a reduction of both the percentage and absolute number of eosinophils (CD11c^{-}Siglec-F^{+}), although it did not affect the absolute number of AMs (CD11c^{+}Siglec-F^{+}), in OVA-induced asthmatic mice (Fig. 2, G–I). In addition, the production of Th2 cytokines IL-4, IL-5, and IL-13 in BALF (Fig. 2 J), as well as that of serum IgE (Fig. 2 K), were reduced in the OVA-induced AMFR-deficient mice. Similarly, after the papain challenge, eosinophil infiltration was lower in LysM^{Cre}*Amfr*$^{fl/fl}$ mice than in *Amfr*$^{fl/fl}$ mice, whereas AM parameters were comparable between the two groups (Fig. 2, L–N). The production of Th2 cytokines (IL-4, IL-5, and IL-13; Fig. 2 O) and IgE (Fig. 2 P) was also decreased in papain-challenged LysM^{Cre}*Amfr*$^{fl/fl}$ mice compared with their WT counterparts. Collectively, these results demonstrate the essential role of AMFR in promoting asthmatic inflammation, probably by priming eosinophil accumulation and Th2 reaction in allergic asthma.

Macrophage-specific AMFR deficiency reduces allergic asthma inflammation

Our results demonstrated that AMFR was upregulated in AMs of OVA-induced asthma, and that myeloid-specific AMFR deficiency ameliorated asthmatic inflammation. To discard other myeloid cells contributing to the resistance of AMFR-deficient mice to asthma, we purified AMs from LysM^{Cre}*Amfr*$^{fl/fl}$ and *Amfr*$^{fl/fl}$ mice, and then adoptively transferred these AMs into clodronate liposome-treated, OVA-sensitized, *Amfr*$^{fl/fl}$ mice. After successful adoptive transfer of AMs (Fig. S3, A and B), these mice were challenged with OVA to establish the asthma model (Fig. 3 A), and evaluate inflammation. Adoptive transfer of *Amfr*$^{-/-}$ AMs prevented OVA-induced lung tissue damage, with significantly fewer infiltrating inflammatory cells and BALF protein compared with results from mice transferred with *Amfr*$^{+/+}$ AMs (Fig. 3, B and C). Accordingly, adoptive transfer of *Amfr*$^{-/-}$ AMs also resulted in decreased tissue damage and glycogen accumulation, compared with that observed in mice receiving *Amfr*$^{+/+}$ AMs (Fig. 3 D). Furthermore, eosinophil accumulation (Fig. 3, E–G), together with production of Th2 cytokines (Fig. 3 H) and IgE (Fig. 3 I), were lower in mice transferred with *Amfr*$^{-/-}$ AMs compared with mice transferred with WT control AMs. Therefore, our results support that AMFR expression in AMs is essential to asthmatic pathogenesis.

AMFR potentiates allergic asthma inflammation through upregulation of GM-CSF

We illustrated above the intrinsic role of AMFR in two allergic asthma induction models. To determine how AMFR affected eosinophilic and Th2 inflammation in asthma, we identified several significant pathways, which were closely associated with cytokine activity (such as "chemokine signaling pathway," "cytokine-cytokine receptor interaction," and "Th1 and Th2 cell differentiation"), based on the KEGG pathway analysis in Fig. 1. To further elucidate which cytokine-related genes were significantly altered in asthmatic mice upon deletion of AMFR, we examined several asthma-related genes by quantitative real-time PCR (qRT-PCR; Table S5). Among these genes, *Csf2* was strongly induced in OVA-challenged mice, whereas AMFR deficiency most effectively blocked *Csf2*, with less affecting other eosinophil-attracting cytokines, including *Ccl3*, *Ccl5*, *Ccl17*, *Ccl22*, and *Ccl24* (Fig. 4 A). Furthermore, we detected that the protein expression of GM-CSF in AMs from OVA-induced LysM^{Cre}*Amfr*$^{fl/fl}$ mice was lower compared with *Amfr*$^{fl/fl}$ OVA mice (Fig. 4, B–D). Because GM-CSF contributes to eosinophil- and Th2 cell–mediated responses in allergic diseases (Nobs et al., 2019), we hypothesized that loss of AM-derived GM-CSF resulted in impaired eosinophil accumulation and Th2 cell reaction in LysM^{Cre}*Amfr*$^{fl/fl}$ mice. To test this hypothesis, we challenged LysM^{Cre}*Amfr*$^{fl/fl}$ mice

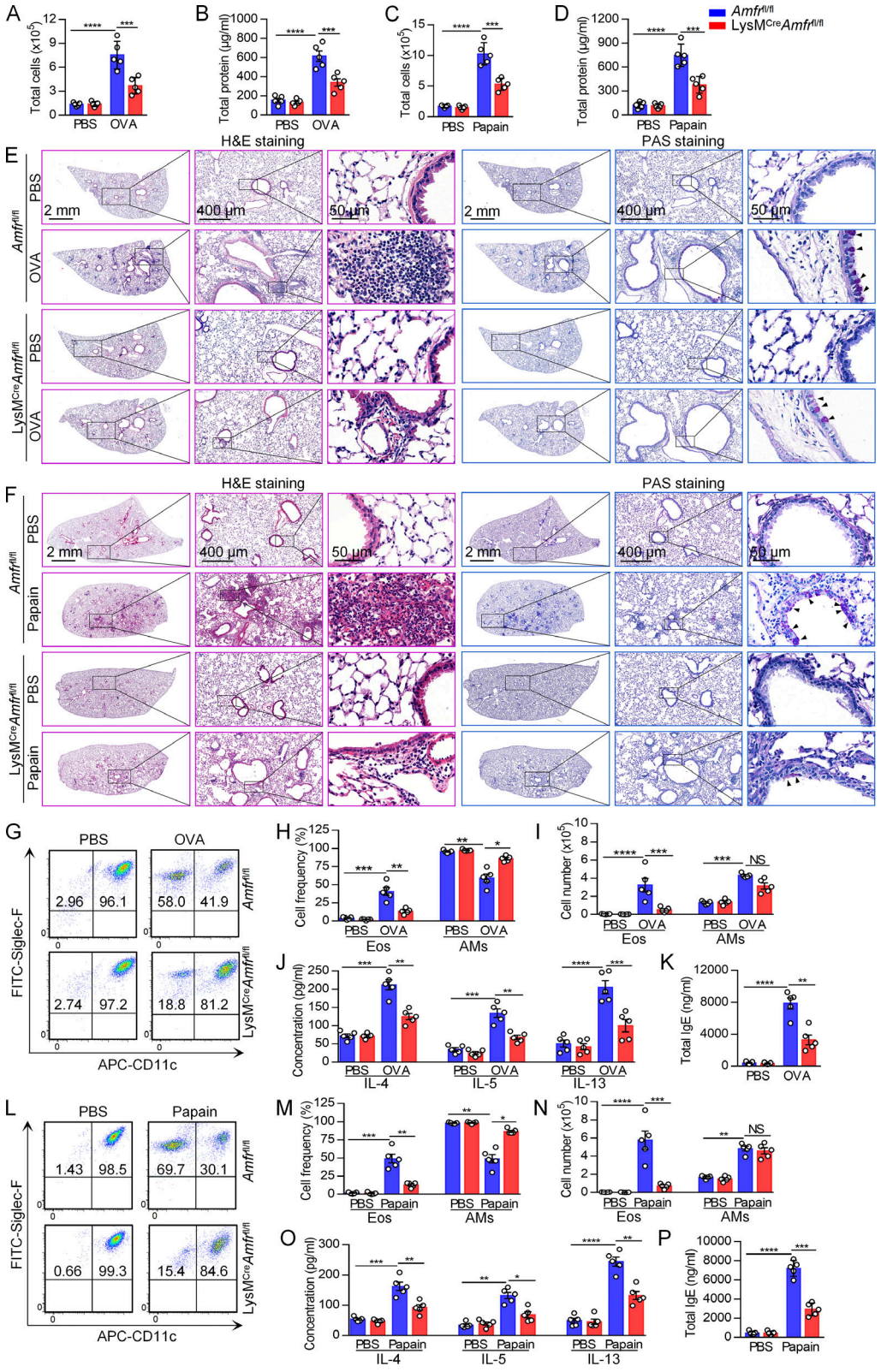

Figure 2. **AMFR promotes eosinophil accumulation and Th2 reaction in allergic asthma induced by OVA or papain. (A–D)** Total cell numbers and total protein concentrations in BALF in OVA- or papain-induced asthma. **(E and F)** Histological analysis of lung sections stained with H&E or PAS in OVA- or papain-induced asthma. Arrowheads indicate goblet cells containing mucus (magenta). Scale bars: 2 mm, 400 μm, and 50 μm. **(G and L)** BALF cells were stained with APC-CD11c and FITC-Siglec-F and assessed by flow cytometry. Eosinophils (Eos, $CD11c^{-}Siglec\text{-}F^{+}$) and alveolar macrophages (AMs, $CD11c^{+}Siglec\text{-}F^{+}$) were identified. **(H, I, M, and N)** Percentages and absolute numbers of eosinophils and AMs in BALF. **(J and O)** ELISA for IL-4, IL-5, and IL-13 in BALF. **(K and P)** ELISA for serum IgE. Numbers in flow plots indicate percentages. Data shown are representative of three independent experiments (E, F, G, and L). Each symbol represents an individual mouse (A–D, H–K, and M–P). Data are presented as mean ± SD from one representative of three independent experiments (n = 5 mice per group per experiment). *, P < 0.05; **, P < 0.01; ***, P < 0.001; ****, P < 0.0001 (two-way ANOVA with Tukey's post hoc analysis, A–D, H–K, and M–P).

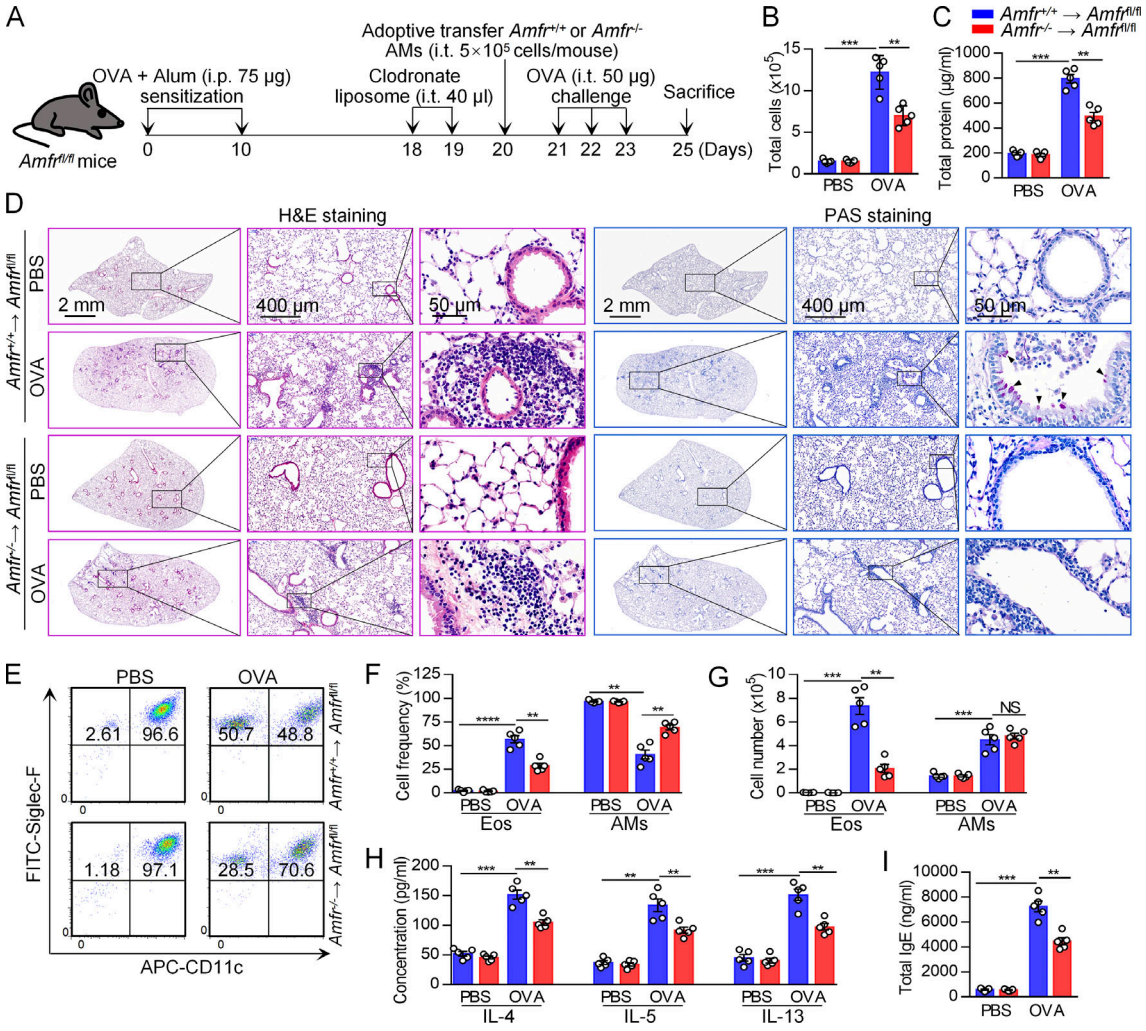

Figure 3. **Macrophage-specific AMFR deficiency reduces allergic asthma inflammation. (A)** Schematic graph of adoptive transfer of AMs, as described in Materials and methods. The *Amfr*$^{fl/fl}$ mice were sensitized with OVA, followed by treatment with 40 μl of clodronate liposome i.t. for two successive days (days 18 and 19). On day 20, the sensitized *Amfr*$^{fl/fl}$ mice treated with clodronate liposome were adoptively transferred with *Amfr*$^{+/+}$ or *Amfr*$^{-/-}$ AMs (*Amfr*$^{+/+}$ → *Amfr*$^{fl/fl}$, *Amfr*$^{-/-}$ → *Amfr*$^{fl/fl}$) at a density of 5 × 10^5 cells/mouse (40 μl), respectively, and then challenged with either PBS or OVA as described before. **(B and C)** Total cell number and total protein concentration in BALF. **(D)** Histopathology of lungs stained with H&E or PAS. Scale bars: 2 mm, 400 μm, and 50 μm. **(E)** Flow cytometry analysis of eosinophils (Eos, CD11c$^-$Siglec-F$^+$) and AMs (AMs, CD11c$^+$Siglec-F$^+$) in BALF. **(F and G)** Percentages and absolute cell numbers of eosinophils and AMs in BALF. **(H)** ELISA for IL-4, IL-5, and IL-13 in BALF. **(I)** ELISA for serum IgE. Numbers in flow plots indicate percentages. Data shown are representative of three independent experiments (D and E). Each symbol represents an individual mouse (B, C, and F–I). Data are presented as mean ± SD from one representative of three independent experiments (n = 5 mice per group per experiment). **, P < 0.01; ***, P < 0.001; ****, P < 0.0001 (two-way ANOVA with Tukey's post hoc analysis, B, C, and F–I).

intranasally with recombinant GM-CSF (Fig. 4 E) and found that this treatment significantly increased OVA-induced asthmatic inflammation, as evidenced by increased total cell number (Fig. 4 F) and protein concentration (Fig. 4 G) in BALF. Infiltrating inflammatory cells, goblet cell hyperplasia, and mucus production were also increased in LysM^{Cre}*Amfr*$^{fl/fl}$ mice supplementing with GM-CSF, as evaluated by H&E and PAS staining, respectively (Fig. 4 H). Additionally, LysM^{Cre}*Amfr*$^{fl/fl}$ mice receiving GM-CSF intratracheally (i.t.) showed an increase in eosinophil percentage and number (Fig. 4, I–K), Th2 cytokines (Fig. 4 L) in BALF, and serum IgE (Fig. 4 M). To further identify whether GM-CSF directly promoted eosinophil migration in vivo, we i.t. administered chitin, a potent inducer of innately driven eosinophilia (Reese et al., 2007). Similar to OVA-induced asthmatic mice, 48 h after treatment, eosinophil infiltration was significantly alleviated in AMFR-knockout mice compared with WT control mice, while intranasal challenge of LysM^{Cre}*Amfr*$^{fl/fl}$ mice with recombinant GM-CSF boosted lung eosinophil accumulation in vivo (Fig. S4). In conclusion, these findings indicate that AMFR regulates allergic inflammation and potentiates eosinophil accumulation by promoting AM-derived GM-CSF production.

AMFR positively regulates TSLP-induced production of GM-CSF by targeting on CIS

Because the complex inflammatory microenvironment is a potent inducer of GM-CSF during the pathogenesis of allergy asthma, and TSLP is at the top of this inflammatory cascade (Lai et al., 2020; Lambrecht et al., 2019), we investigated GM-CSF

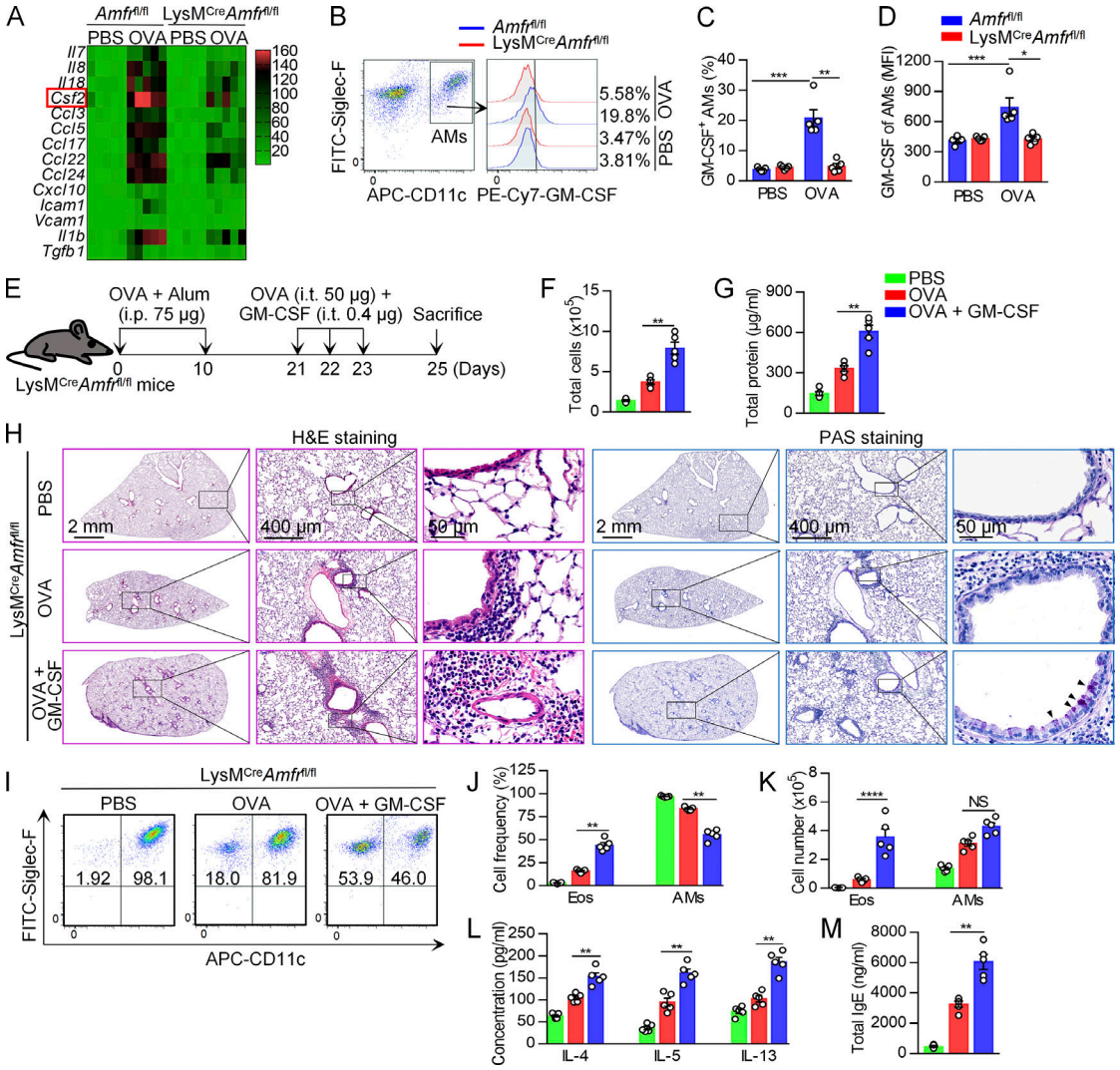

Figure 4. **AMFR potentiates allergic asthma inflammation through upregulation of GM-CSF. (A)** Heatmap summarizing the expression of selected signature genes in lung tissues from *Amfr*$^{fl/fl}$ and LysM^{Cre}*Amfr*$^{fl/fl}$ mice treated with OVA compared with the control using qRT-PCR. **(B–D)** Flow cytometry of GM-CSF in AMs (CD11c$^+$Siglec-F$^+$) from BALF from OVA-induced asthmatic mice and PBS controlled mice. **(C)** Percentage of GM-CSF-producing (GM-CSF$^+$) cells in AMs as gated in B. **(D)** Mean fluorescence intensity (MFI) of GM-CSF$^+$ cells AMs as gated in B. **(E)** Schematic graph of OVA-induced asthma model supplementing with exogenous GM-CSF. **(F and G)** Total cell number and total protein concentration in BALF. **(H)** Histopathology of lung tissues stained with H&E or PAS. Scale bars: 2 mm, 400 μm, and 50 μm. **(I)** Flow cytometry of analysis of eosinophils (Eos, CD11c$^-$Siglec-F$^+$) and AMs (AMs, CD11c$^+$Siglec-F$^+$) in BALF. **(J and K)** Cell percentages and absolute cell numbers of eosinophils and AMs in BALF. **(L and M)** Concentrations of total IL-4, IL-5, and IL-13 in BALF, and serum IgE. Data shown are representative of three independent experiments (B, H, and I). Each symbol represents an individual mouse (C, D, F, G, and J–M). Data are presented as mean ± SD from one representative of three independent experiments (n = 5 mice per group per experiment). *, P < 0.05; **, P < 0.01; ***, P < 0.001; ****, P < 0.0001 (two-way ANOVA with Tukey's post hoc analysis, C and D; one-way ANOVA with Dunn's post hoc analysis, F, G, and J–M).

production in AMFR-deficient macrophages upon TSLP stimulus. As shown in Fig. 5 A, TSLP induced *Csf2* expression in WT BMDMs; however, its efficacy in inducing *Csf2* was reduced in AMFR-deficient BMDMs. Additionally, *Amfr*$^{-/-}$ BMDMs and AMs both exhibited a selective decrease in TSLP-induced protein levels of GM-CSF (Fig. 5, B–G). To test whether AMFR promoted TSLP-induced GM-CSF production in human cells, AMFR-knockdown cells were established in both THP-1 cells and peripheral blood mononuclear cells (PBMCs) using lentivirus-mediated shRNA (Table S6 and Fig. S3, C–F). Consequently, we observed a decreased induction of TSLP-mediated GM-CSF production in AMFR-knockdown THP-1 cells (Fig. 5, H–J) and PBMCs (Fig. 5, L–N). Consistent with the flow data, *CSF2* gene transcription by TSLP was significantly higher in scramble control cells than in AMFR-knockdown THP-1 cells (Fig. 5 K) and PBMCs (Fig. 5 O). Collectively, these results suggest that AMFR promotes GM-CSF release in macrophages following TSLP stimulation.

As AMFR was specifically required for TSLP-induced GM-CSF production, we next assessed the effect of AMFR on TSLP signaling. We first found that TSLP could induce AMFR expression in macrophages (Fig. 5, P and Q), in line with the upregulation of AMFR illustrated in Fig. 1. In addition, we observed that TSLP-induced phosphorylation of STAT5 was significantly attenuated in AMFR-deficient BMDMs compared with that in WT BMDMs,

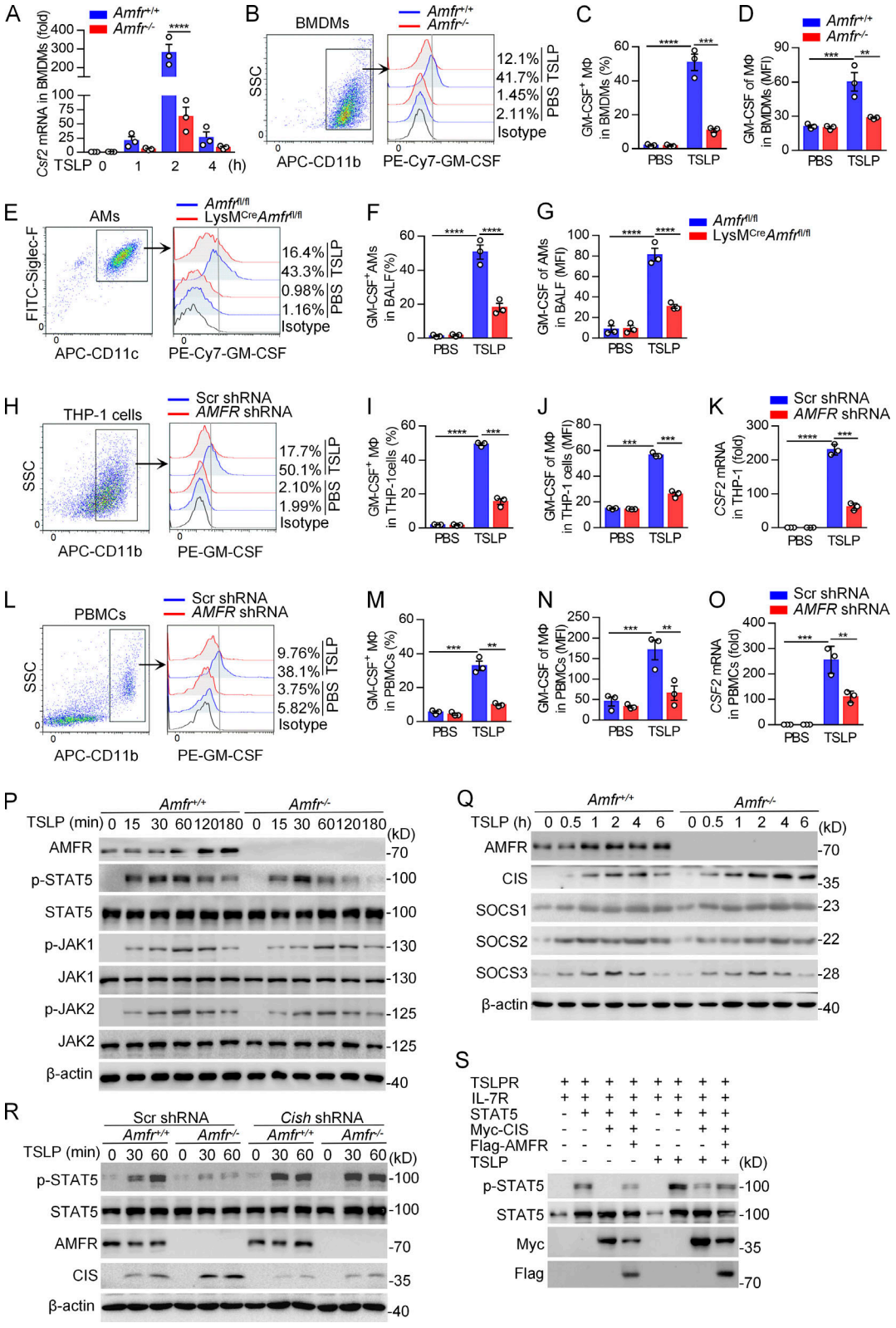

Figure 5. **AMFR positively regulates TSLP-induced production of GM-CSF by targeting CIS. (A)** mRNA levels of GM-CSF in *Amfr*$^{+/+}$ and *Amfr*$^{-/-}$ BMDMs under TSLP (10 ng/ml) stimulation as measured using qRT-PCR. **(B)** Flow cytometry of GM-CSF in *Amfr*$^{+/+}$ and *Amfr*$^{-/-}$ BMDMs under TSLP stimulation (10 ng/ml) for 3 h. SSC, side scatter. **(C and D)** Percentage and mean fluorescence intensity (MFI) of GM-CSF-producing cells (GM-CSF^{+}) in BMDMs. **(E)** Flow cytometry of GM-CSF in AMs from *Amfr*$^{fl/fl}$ and LysM^{Cre}*Amfr*$^{fl/fl}$ mice BALF under TSLP stimulation (10 ng/ml) for 3 h. **(F and G)** Percentage and mean fluorescence intensity (MFI) of GM-CSF–producing cells (GM-CSF^{+}) in AMs. **(H–K)** THP-1 cells were transfected with lentivirus-mediated *AMFR* shRNA or Scr shRNA, followed by stimulation with PMA (100 ng/ml) for 24 h to differentiate to macrophages, and then treated with TSLP for 3 h. The protein (H) and mRNA

(K) expression of GM-CSF were measured using flow cytometry and qRT-PCR, respectively. **(I and J)** Percentage and MFI of GM-CSF–producing macrophages in THP-1 cells (gated on $CD11b^+$). **(L–O)** PBMCs were transfected with lentivirus-mediated *AMFR* shRNA or Scr shRNA, and then treated with TSLP (10 ng/ml) for 3 h. The protein (L) and mRNA (O) expression of GM-CSF were measured using flow cytometry and qRT-PCR, respectively. **(M and N)** Percentage and MFI of GM-CSF–producing PBMCs (gated on $CD11b^+$). **(P and Q)** Immunoblot analysis of phosphorylated (p-) STAT5, JAK1, JAK2, total STAT5, JAK1, JAK2, CIS, SOCS1, SOCS2, SOCS3, and β-actin in whole cell lysates of $Amfr^{+/+}$ and $Amfr^{-/-}$ BMDMs stimulated with TSLP (10 ng/ml) at various time points. **(R)** Immunoblot analysis of phosphorylated and total STAT5 protein levels in $Amfr^{+/+}$ and $Amfr^{-/-}$ BMDMs transfected with lentivirus-mediated *Cish* shRNA or Scr shRNA, and 48 h later, stimulated with TSLP (10 ng/ml) at various time points. **(S)** Immunoblot analysis of phosphorylated and total STAT5 in HEK293T cells transfected with various combinations (upper lanes) of plasmids encoding IL-7R, TSLPR, STAT5, Flag-AMFR, and Myc-CIS, and 48 h after transfection, stimulated with TSLP (10 ng/ml) for 60 min. Data are presented as mean ± SD from three independent experiments with biological duplicates in each (A, C, D, F, G, I–K, and M–O) or are representative of three independent experiments (B, E, H, L, and P–S). **, $P < 0.01$; ***, $P < 0.001$; ****, $P < 0.0001$ (two-way ANOVA with Sidak's post hoc analysis, A; two-way ANOVA with Tukey's post hoc analysis, C, D, F, G, I–K, and M–O). Source data are available for this figure: SourceData F5.

while AMFR deficiency did not affect TSLP-induced phosphorylation of JAK1 and JAK2 (Figs. 5 P and S3 G). These results suggest that GM-CSF regulation by AMFR is downstream of JAK1 and JAK2, and probably dependent on the activation of STAT5.

Considering the previous reports stating that the activation of STAT5 was negatively regulated by suppressor of cytokine signaling (SOCS) family proteins (CIS, SOCS1, SOCS2, and SOCS3; Li et al., 2017; Peltola et al., 2004), we next determined the expression of these proteins, and found that TSLP induced a significantly increased accumulation of CIS, but not of SOCS1, SOCS2, or SOCS3, in AMFR-deficient macrophages compared with WT control cells (Figs. 5 Q and S3 H). This finding indicated that AMFR may regulate the activity of STAT5 by targeting on CIS. To explore this point, we did a rescue experiment, in which we silenced CIS expression using lentivirus-mediated *Cish* shRNA (Table S6). Although three different *Cish* shRNAs (*Cish* shRNA 1, 2, and 3) were prepared, it was *Cish* shRNA 2 that most significantly reduced CIS expression at both mRNA and protein levels compared with the scrambled (Scr) shRNA (Fig. S3, I and J). *Cish* shRNA 2 was used for further study, and we indeed found that CIS knockdown restored the TSLP-induced phosphorylation of STAT5 in AMFR-deficient macrophages (Figs. 5 R and S3 K). Additionally, we established an automatic STAT5 activation system, in which IL-7R, TSLPR, STAT5, AMFR, and CIS were transiently expressed in HEK293T cells. We found that increased AMFR expression reduced the expression of CIS, accompanied by increased levels of the phosphorylated STAT5 (Figs. 5 S and S3 L). Taken together, these results suggest that AMFR likely promotes TSLP-induced GM-CSF production and STAT5 activation by downregulating the expression of CIS protein.

Knockdown of CIS restores OVA-induced asthmatic inflammation in myeloid-specific AMFR-deficient mice

To address the causal role of the augmented CIS expression in $Amfr^{-/-}$ macrophages in mediating their considerably diminished asthmatic inflammatory response in vivo, we conducted an additional macrophage adoptive transfer study. Clodronate liposome-treated, OVA-sensitized, recipient $LysM^{Cre}Amfr^{fl/fl}$ mice were i.t. injected with Scr shRNA– or *Cish* shRNA–treated $Amfr^{-/-}$ BMDMs, followed by OVA challenge as previously mentioned (Fig. 6 A). After 24 h of macrophage adoptive transfer, the CIS mRNA and protein levels in pulmonary macrophages were >50% lower in $LysM^{Cre}Amfr^{fl/fl}$ mice receiving CIS-knockdown $Amfr^{-/-}$ BMDMs compared with $LysM^{Cre}Amfr^{fl/fl}$ mice receiving control $Amfr^{-/-}$ BMDMs (Fig. S3, M and N). After OVA challenge, $LysM^{Cre}Amfr^{fl/fl}$ mice adoptively transferred with CIS-knockdown $Amfr^{-/-}$ macrophages suffered from aggravating OVA-induced lung tissue damage, with significantly increased cell number (Fig. 6 B), protein concentration (Fig. 6 C), and higher production of IgE (Fig. 6 D), IL-4, IL-5, and IL-13 (Fig. 6 E) compared with their $LysM^{Cre}Amfr^{fl/fl}$ counterparts adoptively transferred with control $Amfr^{-/-}$ macrophages. In agreement with this, $LysM^{Cre}Amfr^{fl/fl}$ mice adoptively transferred with CIS-knockdown $Amfr^{-/-}$ macrophages also exhibited more infiltrating inflammatory cells and increased glycogen accumulation compared with their $LysM^{Cre}Amfr^{fl/fl}$ counterparts adoptively transferred with control $Amfr^{-/-}$ macrophages (Fig. 6 F). Furthermore, lentivirus-mediated *Cish* shRNA significantly restored the expression of GM-CSF in both OVA-challenged $LysM^{Cre}Amfr^{fl/fl}$ mice in vivo (Fig. 6 G) and TSLP-induced $Amfr^{-/-}$ BMDMs in vitro (Fig. 6, H–J). Taken together, our results illustrate that AMFR modulates asthmatic inflammation and GM-CSF production, which is at least partially dependent on its effect on suppressing CIS expression in macrophages.

AMFR interacts with CIS

Next, we addressed the mechanisms by which the AMFR-induced inhibition of CIS expression mediated asthmatic inflammation. Because AMFR is considered an ER-resident E3 Ub ligase, and we found that AMFR deficiency enhanced TSLP-induced CIS accumulation (Fig. 5 Q), we hypothesized that AMFR deficiency may counteract the CIS Ub system. To test this, we first examined whether AMFR interacted with CIS. Our results showed that AMFR specifically associated with CIS (Fig. 7 A), but not with STAT5 isoform a or b, SCOS1, SOCS2, or SOCS3 (Fig. S5, A–E) in the HEK293T cell overexpression system. Additionally, the interaction between endogenous AMFR and CIS was enhanced upon TSLP stimulation (Fig. 7 B). Then, to map the specific interaction region of CIS with AMFR, we generated three AMFR mutants—AMFR ΔRING (RING finger motif deletion), AMFR ΔCUE (CUE domain deletion), AMFR ΔVIM (p97/VCP-interacting motif deletion)—and two CIS truncation mutants—CIS ΔSH2 (SH2 domain deletion) and CIS ΔSOCS (SOCS box deletion)—according to their functional motifs. As shown in Fig. 7, C and D, the interaction of AMFR with CIS was blocked in either AMFR ΔCUE mutant or CIS ΔSH2 mutant, thus indicating that the CUE domain in AMFR and the SH2 domain in CIS were indispensable for their interaction.

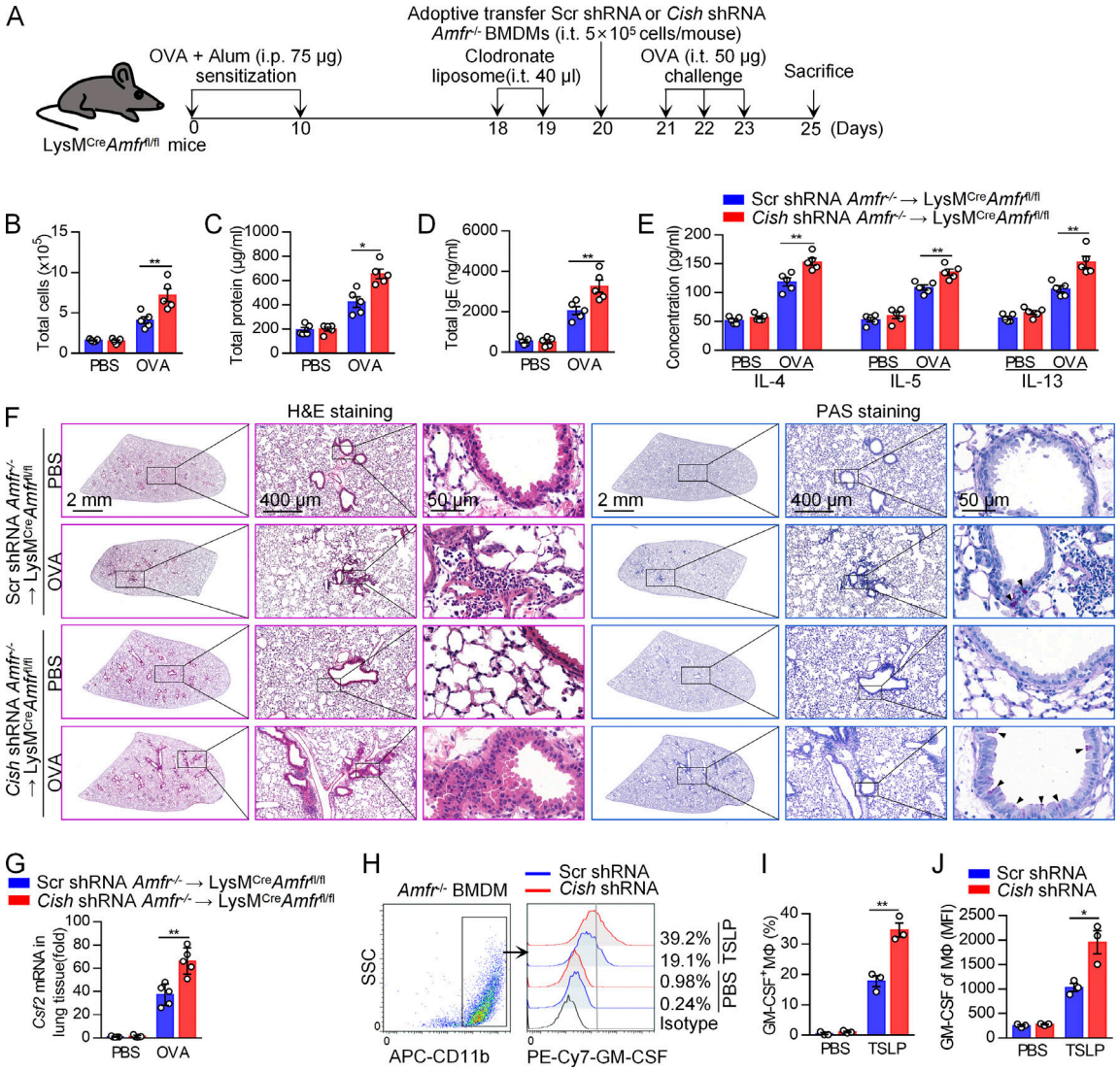

Figure 6. **Knockdown of CIS restores OVA-induced asthmatic inflammation in myeloid-specific AMFR-deficient mice. (A)** Schematic graph of the macrophage adoptive transfer described in Materials and methods. OVA-sensitized recipient LysM^{cre}*Amfr*$^{fl/fl}$ mice under i.t. treatment with clodronate liposome were i.t. injected with *Amfr*$^{-/-}$ BMDMs infected with either Scr shRNA or *Cish* shRNA (Scr shRNA *Amfr*$^{-/-}$ → LysM^{Cre}*Amfr*$^{fl/fl}$, *Cish* shRNA *Amfr*$^{-/-}$ → LysM^{Cre}*Amfr*$^{fl/fl}$) at a density of 5 × 10^5 cells/mouse (40 µl) and then challenged with either PBS or OVA as in previous experiments. **(B–E)** Total cell number (B), protein concentration (C), IgE (D), and IL-4, IL-5, and IL-13 (E) were measured from each group of mice. **(F)** Histopathology of lung tissues stained with H&E or PAS. Scale bars: 2 mm, 400 µm, and 50 µm. **(G)** mRNA expression of GM-CSF in lung tissues of mice was measured using qRT-PCR. **(H)** Flow cytometry of GM-CSF–producing cells in *Amfr*$^{-/-}$ BMDMs transfected with either lentivirus-mediated *Cish* shRNA or Scr shRNA under stimulation of TSLP (10 ng/ml) for 3 h. SSC, side scatter. **(I)** Percentage of GM-CSF–positive cells in BMDMs. **(J)** MFI of GM-CSF–producing cells in macrophages. Data shown are representative of three independent experiments (F and H). Each symbol represents an individual mouse, and data are presented as mean ± SD from one representative of three independent experiments (*n* = 5 mice per group per experiment; B–E and G). Each symbol represents data from an independent experiment, and data are presented as mean ± SD from one representative of three independent experiments with biological duplicates in each (*n* = 3; I and J). *, P < 0.05; **, P < 0.01 (two-way ANOVA with Tukey's post hoc analysis, B–E, G, I, and J).

As AMFR has been reported to be located on the ER (Joshi et al., 2017), we next tried to determine the subcellular localization of CIS and AMFR by confocal microscopy assay. As shown in Fig. 7 E, CIS maintained at a very low level in resting BMDMs. Upon TSLP stimulation, CIS was upregulated and largely colocalized with AMFR. Moreover, CIS and AMFR were shown to be localized together using an ER-Tracker (an ER-specific dye) in TSLP activated BMDMs. In addition, although overexpression of AMFR (WT, AMFR ΔRING, or AMFR ΔVIM) and CIS (WT or CIS ΔSOCS) in HEK293T cells showed the colocalization of CIS and AMFR on ER, overexpressed AMFR ΔCUE or CIS ΔSH2 did not (Fig. 7, F and G). Collectively, our results demonstrate that the CUE domain of AMFR interacts with the SH2 domain of CIS, resulting in the generation of an AMFR-CIS complex on the ER.

AMFR regulates TSLP signaling pathway by promoting degradation and K48-linked polyubiquitination of CIS

Considering that AMFR regulated TSLP-induced CIS protein accumulation and interacted directly with CIS (Figs. 5 and 7), we next evaluated whether AMFR could regulate the degradation of

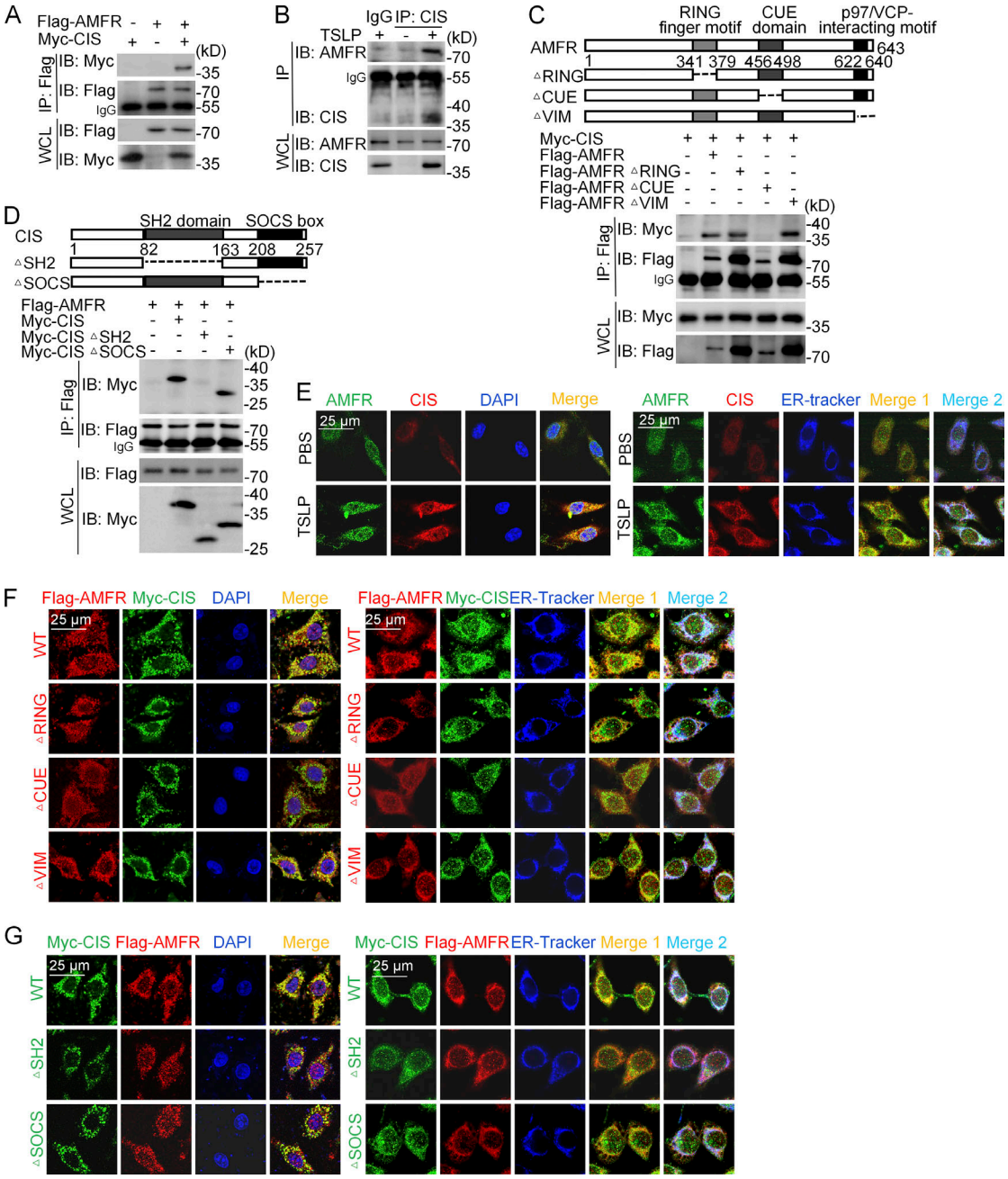

Figure 7. **AMFR interacts with CIS. (A)** Immunoprecipitation (IP) and immunoblot (IB) analysis of lysates of HEK293T cells transfected with various combinations (upper lanes) of plasmids encoding Flag-AMFR and Myc-CIS. WCL, whole-cell lysate. **(B)** Immunoprecipitation and immunoblot analysis of BMDMs stimulated with TSLP (10 ng/ml), followed by IP with anti-CIS Ab and IgG as negative control. **(C)** Immunoprecipitation and immunoblot analysis of lysates of HEK293T cells transfected with Myc-CIS, plus Flag-AMFR or Flag-AMFR mutants—namely AMFR ΔRING (RING finger motif deletion), AMFR ΔCUE (CUE domain deletion), or AMFR ΔVIM (p97/VCP-interacting motif deletion)—followed by IP with the anti-Flag Ab. **(D)** Immunoprecipitation and immunoblot analysis of HEK293T cells transfected with Flag-AMFR, plus Myc-CIS, or Myc-CIS mutants—namely CIS ΔSH2 (SH2 domain deletion) or CIS ΔSOCS (SOCS box deletion)—followed by IP with the anti-Flag Ab. **(E)** Confocal microscopy imaging of BMDMs stimulated with TSLP (10 ng/ml) and labeled with antibodies for AMFR (green) and CIS (red), along with DAPI and ER tracker, respectively. Merge, AMFR + CIS + DAPI; merge 1, AMFR + CIS; and merge 2, AMFR + CIS + ER-tracker. **(F)** Confocal microscopy imaging of HeLa cells expressing Flag-AMFR, Flag-AMFR mutant vectors (red), and Myc-CIS (green) with antibodies to the appropriate protein, along with DAPI and ER tracker, respectively. Merge, Flag-AMFR + Myc-CIS + DAPI; merge 1, Flag-AMFR + Myc-CIS; and merge 2, Flag-AMFR + Myc-CIS + ER-tracker. **(G)** Confocal microscopy imaging of HeLa cells expressing Myc-CIS, Myc-CIS mutant vectors (green), and Flag-AMFR (red) with antibodies to the appropriate protein, along with DAPI and ER tracker, respectively. Merge, Flag-AMFR + Myc-CIS + DAPI; merge 1, Flag-AMFR + Myc-CIS; and merge 2, Flag-AMFR + Myc-CIS + ER-tracker. Blue indicates cell nucleus DAPI or ER-tracker. Scale bar: 25 μm. Data shown are representative of three independent experiments (A–G). Source data are available for this figure: SourceData F7.

CIS through the proteasome pathway. Hence, we transfected the same amount of CIS plasmid accompanied by different amounts of AMFR plasmid into HEK293T cells. CIS expression was substantially reduced with increased levels of AMFR, while the abundance of CIS was restored in the presence of the proteasome inhibitor MG132, which indicated that AMFR mediated CIS degradation via the Ub-proteasome system (Figs. 8 A and S5 F). We then studied the direct effect of AMFR on CIS polyubiquitination in vitro. To this purpose, the Myc-tagged CIS plasmid was cotransfected with the HA-tagged Ub and Flag-tagged AMFR plasmids into HEK293T cells. Our data revealed that overexpression of AMFR significantly induced CIS ubiquitination, whereas overexpression of three AMFR-truncated mutants failed to enhance CIS polyubiquitination in HEK293T cells. This is likely indicative of the RING finger motif, CUE domain, and p97/VCP-interacting motif being involved in the ubiquitination of CIS by AMFR (Fig. 8 B).

Next, we assessed AMFR-mediated polyubiquitination of CIS under physiological conditions. As shown in Fig. 8 C, stimulation with TSLP caused CIS ubiquitination in WT BMDMs (but not in AMFR-deficient BMDMs), suggesting an important role for AMFR in the ubiquitination of CIS downstream of the TSLP pathway. To unravel which polyubiquitin linkage on CIS was regulated by AMFR, plasmids for WT Ub (containing all seven lysine residues), sequential Ub substitution mutants (K6, K11, K27, K29, K33, K48, and K63, with only one of the seven lysine residues retained as lysine, and the other six replaced with arginine), CIS, and AMFR were transfected into HEK293T cells. The results demonstrated that AMFR significantly promoted K48-linked polyubiquitination of CIS (Fig. 8 D), Consistently, CIS could not be ubiquitinated when mutant Ub plasmid K48R (substitution of the lysine residue at position 48 with arginine) was transfected into this system (Fig. 8 E). These data indicate that AMFR mediates K48-linked polyubiquitination of CIS.

Finally, to determine the specific sites of AMFR-mediated ubiquitination in CIS, we identified all lysine sites (Lys59, Lys72, Lys98, Lys121, Lys188, and Lys208) in CIS and substituted them with arginine to create six single-site mutants (CIS K59R, K72R, K98R, K121R, K188R, and K208R). Although the K98R mutant located in SH2 domain could still bind to AMFR (Fig. S5 G), this mutation almost completely blocked AMFR-induced ubiquitination and degradation of CIS, suggesting that Lys98 was required for AMFR-mediated CIS ubiquitination (Fig. 8, F and G; and Fig. S5 H). Furthermore, the inhibitory effect of AMFR on CIS-reduced phosphorylation of STAT5 was impaired by the K98R mutation of CIS (Figs. 8 H and S5 I). In addition, GM-CSF production induced by TSLP was also hampered by overexpression of the K98R CIS mutant compared with CIS WT in *Amfr*$^{+/+}$ BMDMs (Fig. 8, I–K).

In conclusion, Lys98 of CIS was essential for AMFR-mediated ubiquitination and degradation of CIS. Hence, our results reveal a modulatory role of AMFR in regulating TSLP-induced GM-CSF production, in which increased expression of AMFR promotes K48-linked ubiquitination and degradation of CIS.

Discussion

AMs are crucial to environmental allergen-induced airway inflammation in asthma. However, the precise molecular mechanisms of AMs mediating inflammatory immunity response in asthma remain speculative. In the present study, we report that AMFR, an E3 Ub ligase, was upregulated in AMs of allergic asthmatic mice. Through myeloid cell–restricted deletion of AMFR, we demonstrated that AMFR deficiency resulted in attenuated inflammatory and asthmatic responses via controlling AMs. Moreover, we found that AMFR was required for macrophage, eosinophil, and Th2 cell cross talk through regulating GM-SCF expression in AMs via Ub modification of TSLP signaling. Thus, our study offers a novel insight into how asthmatic inflammation is influenced by AMs, and how AMs or AM-derived cytokines could emerge as potential targets for intervening allergic asthma.

During allergic inflammation, the cytokines produced by epithelial cells or allergen-specific Th2 cells are largely held responsible for orchestrating the various features of asthma (Fahy, 2015). Previous studies have highlighted macrophages as effector cells downstream of Th2 cells via type 2 cytokines (Walker and McKenzie, 2018). Conversely, we identified eosinophils and Th2 cells as effector cells for AMs, probably through GM-CSF production. Particularly in the lung, GM-CSF has been implicated as a mediator in asthmatic pathogenesis (Schuijs et al., 2015). For example, GM-CSF has been shown to induce the recruitment, accumulation, activation, and migration of eosinophils and to promote a DC and T cell inflammatory circuit in GM-CSF receptor α-deficient (*Csf2ra*$^{-/-}$) mice, with a reconstitution of normal AM compartment (Nobs et al., 2021). However, our data showed that AMFR deficiency could significantly decrease the production of cytokines in AMs in the asthmatic microenvironment.

Another interesting finding was that the production of GM-CSF in asthmatic AMs from LysM^{Cre}*Amfr*$^{fl/fl}$ was significantly diminished, while supplementing with GM-CSF restored the asthmatic symptoms, as well as Th2, and eosinophilic inflammation in OVA-induced allergic airway inflammation in LysM^{Cre}*Amfr*$^{fl/fl}$ mice. Thus, our results indicated that the regulatory effect of AMFR in asthma was mainly through regulating the release of AM-derived GM-CSF. A previous study reported that alveolar epithelial type 2 cell–derived GM-CSF was essential for the development and homeostasis of AMs (Gschwend et al., 2021). Our data showed no significant differences in macrophage maturation between LysM^{Cre}*Amfr*$^{fl/fl}$ mice and *Amfr*$^{fl/fl}$ mice (not depicted), which indicated that AM-derived GM-CSF was dispensable for macrophage development in the lung but essential for mediating the cross talk between AMs and eosinophils and Th2 cells as a tissue-specific modulator in a paracrine manner.

Ubiquitination is an important physiological pathway that mediates numerous biological processes (Hu and Sun, 2016). Although it is involved in inflammation through the degradation of various target proteins participating in intracellular signaling transduction, gene expression, antigen receptor cross-linking, and cytokine receptors, among others (Jiang and Chen, 2011; Liu et al., 2013), the role of the Ub pathway in AMs in asthma has not been reported to date. Here, we identified that E3 Ub ligase AMFR was upregulated in AMs from asthmatic mice. As a membrane-bound protein, AMFR was initially identified as a cell

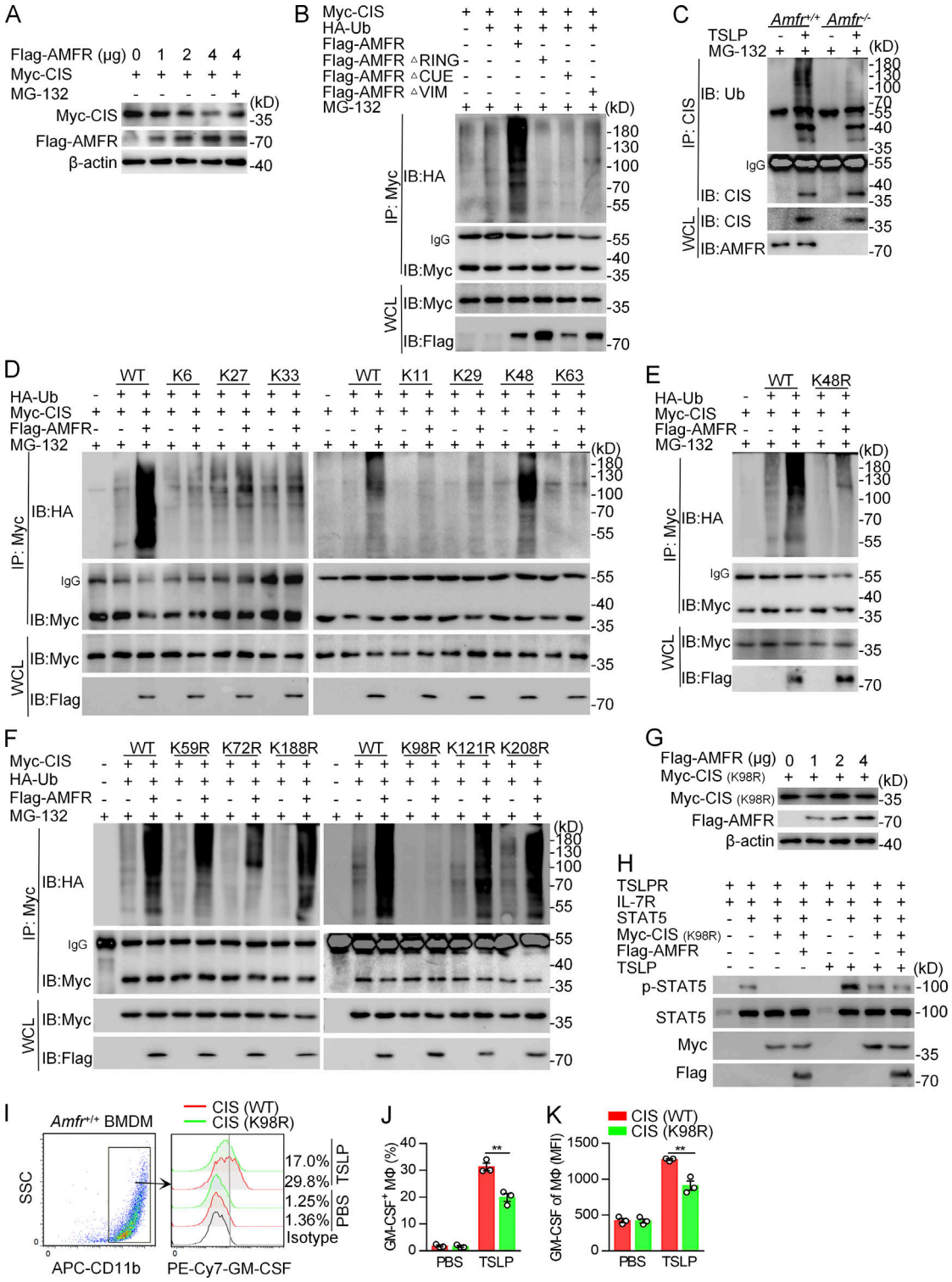

Figure 8. **AMFR promotes the degradation and K48-linked polyubiquitination of CIS. (A)** Immunoblot (IB) analysis of CIS protein expression in HEK293T cells transfected with Myc-CIS and different amounts of Flag-AMFR. The proteasome inhibitor MG132 was added to treat the cells for 4 h, if necessary. β-Actin acted as a loading control. WCL, whole-cell lysate. **(B)** Immunoprecipitation (IP) and immunoblot (IB) analysis of ubiquitination of CIS in HEK293T cells cotransfected with Myc-CIS, HA-Ub, along with Flag-AMFR, Flag-AMFR ΔRING, Flag-AMFR ΔCUE, or Flag-AMFR ΔVIM. **(C)** Immunoprecipitation and immunoblot analysis of ubiquitination of CIS in *Amfr*$^{+/+}$ and *Amfr*$^{-/-}$ BMDMs stimulated with TSLP (10 ng/ml) for 4 h. **(D and E)** HEK293T cells were transfected with Myc-CIS and Flag-AMFR, along with HA-Ub or its mutants (K6, K11, K27, K29, K33, K48, K63, and K48R). Cell lysates were subjected to immunoprecipitation by the anti-Myc Ab, and then immunoblotted with the indicated antibodies. **(F)** Myc-CIS or its mutants (K59R, K72R, K98R, K121R, K188R, and K208R) were individually transfected into HEK293T cells, along with Flag-AMFR and HA-Ub. Cell lysates were subjected to immunoprecipitation by the anti-Myc Ab, and then immunoblotted with the indicated antibodies. **(G)** Immunoblot analysis of CIS protein levels in HEK293T cells transfected with Myc-CIS (K98R) with different amounts of Flag-AMFR. β-Actin acted as a loading control. **(H)** Immunoblot analysis of phosphorylated and total STAT5 in HEK293T cells

transfected with various combinations (upper lanes) of plasmids encoding IL-7R, TSLPR, STAT5, Flag-AMFR, and Myc-CIS (K98R), and 48 h later, stimulated with TSLP (10 ng/ml) for 60 min. **(I)** Flow cytometry of GM-CSF–producing cells in BMDMs under stimulation of TSLP (10 ng/ml) for 3 h. SSC, side scattert. **(J and K)** Percentage and MFI of GM-CSF–positive cells in macrophages as presented in I. MFI, mean fluorescence intensity. Data are representative of three independent experiments (A–I) or are presented as mean ± SD from three independent experiments with biological duplicates in each (J and K). **, P < 0.01 (two-way ANOVA with Tukey's post hoc analysis, J and K). Source data are available for this figure: SourceData F8.

surface receptor for cytokines such as autocrine motility factor (AMF) and CCL1, which participates in establishing interaction between a cell and its external environment (Fairbank et al., 2009; Liu et al., 2021). In addition, subsequent studies revealed that apart from its presence over the cell surface, AMFR was also distributed throughout the cytoplasm in vesicular and tubular structures, especially on ER membranes (Wang et al., 2014). The ER-located AMFR acted as an E3 Ub ligase involved in mediating the ERAD pathway (Fang et al., 2001). In our study, we found that AMFR was mainly located in the ER, and it was shown to promote TSLP-induced phosphorylation of STAT5 through recruiting CIS to ER for ubiquitination and degradation. Thus, combined with a previous study that showed the ER-located AMFR to recruit STING (stimulator of interferon gene) for polyubiquitination (Wang et al., 2014), we think AMFR is more likely an ER-resident E3 Ub ligase that regulates the function of macrophages, and its cell surface function as receptor for AMF and CCL1 is more likely concentrated on cancer cells and fibroblasts. Collectively, our results linked the Ub pathway to the function of AMs in the development and exacerbation of asthma. Therefore, AMFR expression in macrophages could be used as a clinical prognostic biomarker of asthma development and progression, and to evaluate the risk of asthma. Furthermore, accurate macrophage modifiers targeting AMFR may provide a new direction for allergic disease therapies in the future.

Importantly, we identified the TSLP signaling regulator CIS as a checkpoint controller for AMFR function in macrophages. TSLP is an alarmin cytokine that plays a major role in the pathology of asthma (Al-Shami et al., 2005). Drugs that target TSLP and TSLP-mediated signaling, such as tezepelumab, a humanized anti-TSLP mAb, have been shown to improve lung function compared with placebo in asthmatic patients (Corren et al., 2017). Here, we found that TSLP significantly induced GM-CSF expression in macrophages, and that AMFR deficiency led to decreased TSLP-induced GM-CSF expression, with specifically enhanced expression of CIS. A member of the SOCS family, CIS has been reported to act as a negative-feedback inhibitor of TLSP signaling (Isaksen et al., 1999; Palmer and Restifo, 2009). It is demonstrated that TSLP induces a rapid, but transient, upregulation of CIS (Isaksen et al., 1999), but the degradation mechanism has never been reported. In our study, we found that AMFR directly bound to the SH2 domain of CIS in a CUE domain–dependent manner. Furthermore, Lys98 of CIS was further identified as the site of ubiquitination. Thus, our findings fundamentally showed that AMFR promoted GM-CSF production in macrophages by degradation of CIS but not STAT5, SOCS1, SOCS2, or SOCS3. As CIS is also involved in the intracellular cytokine signal cascades such as IL-2, IL-3, and IL-15 (Delconte et al., 2016; Yang et al., 2013), it is worthwhile to explore whether AMFR also modulates the degradation of CIS in these signalings in the future.

In conclusion, our results demonstrate that AMFR binds to CIS and regulates ubiquitination of CIS, thereby fine-tuning TSLP-STAT5 signaling in AMs, which contributes to the development of Th2 response, accumulation of eosinophils, and promotion of allergic airway inflammation (Fig. 9).

Materials and methods

Mice

Myeloid-specific AMFR-deficient ($LysM^{Cre}Amfr^{fl/fl}$) mice were generated by breeding Lysozyme M-Cre mice (Jackson Laboratory) with $Amfr^{fl/fl}$ mice (clone B000405; KOMP Repository). Cre-negative $Amfr^{fl/fl}$ littermates were used as controls. Primers for genotyping are shown in Table S4. All mice were kept in pathogen-free facilities at the Shanghai Jiao Tong University (Shanghai, China). All animal experiments were approved by the Animal Care and Use Committee of Shanghai Jiao Tong University and were performed according to "Animal Management Regulations" (revised 2017) formulated by the National Science and Technology Commission.

Reagents

OVA (A5503), papain (76216), chitin (C9752), collagenase D (11088866001), and DNase I (10104159001) were obtained from Sigma-Aldrich. The Imject Alum adjuvant (77161) and ER-TrackerTM Blue-White DPX (E12353) were purchased from Thermo Fisher Scientific. Clodronate liposomes (CP-005-005) were purchased from Liposoma. The recombinant murine (555-TS) and human (1398-TS) TSLP cytokines were purchased from R&D. Recombinant murine GM-CSF (315-03) and M-CSF (315-02) were from PeproTech. The anti-AMFR (ab76841) antibody was obtained from Abcam. The anti-CIS antibody (sc-166326) was obtained from Santa Cruz Biotechnology. The anti-CD68 antibody (14-0681-80) was purchased from Invitrogen Thermo Fisher Scientific. Antibodies for Myc-Tag (2272S and 2276S), Flag-Tag (14793S), HA-Tag (3724S), β-actin (8457S), Ub (3936S), STAT5 (94205S), phospho-STAT5 (9351L), phospho-JAK1 (74129T), JAK1 (3344T), phospho-JAK2 (8082T), JAK2, (3230T), SOCS1 (3950T), SOCS2 (2779P), SOCS3 (2932P), Alexa Fluor 594 anti-mouse IgG (8890S), and Alexa Fluor 488 anti-rabbit IgG (4412S) were obtained from Cell Signaling Technology. The secondary antibodies peroxidase-conjugated anti-rabbit (111-035-003) and anti-mouse (115-035-003) were purchased from Jackson ImmunoResearch Laboratories. The flow cytometry antibodies, including APC anti-mouse CD11c (117310), FITC anti-mouse Siglec-F (155504), PE anti-mouse Siglec-F (155506), APC anti-mouse/human CD11b (101212), PE/Cyanine7 anti-mouse CD45 (103114), PerCP/Cyanine5.5 anti-mouse CD64 (139307),

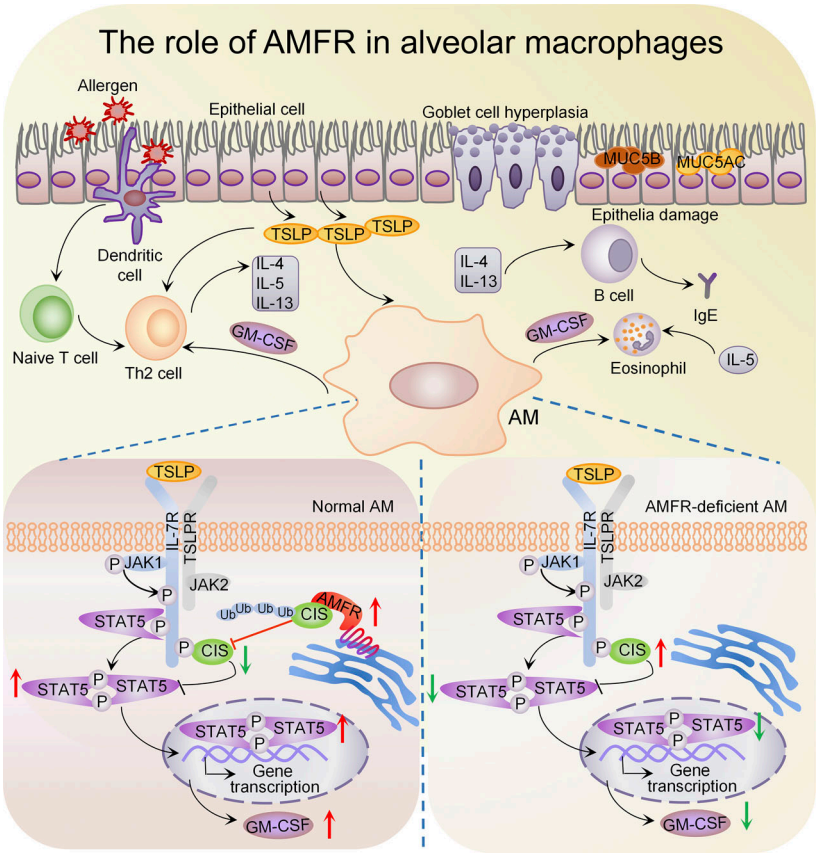

Figure 9. **Schematic diagram for the role of AMFR in AMs.** AMFR regulates asthmatic inflammation by promoting the production of GM-CSF, leading to recruitment, accumulation, and activation of eosinophils and Th2 cells in the airway. Under TSLP stimulation, AMFR, whose expression is upregulated in AMs, directly binds to and destabilizes CIS, resulting in augmented activation of STAT5 and GM-CSF production.

APC/Fire 750 anti-mouse Ly-6G (127652), Brilliant Violet 650 anti-mouse F4/80 (123149), Brilliant Violet 421 anti-mouse/human CD11b (101235), FITC anti-mouse I-A/I-E (MHC class II; 107605), PE anti-human GM-CSF (502305), and PE/Cyanine7 anti-mouse GM-CSF (505411), were from BioLegend. The BCA protein assay kit (P0012S) and DAPI (C1002) were obtained from Beyotime.

Cell culture and differentiation

BMDMs were isolated from WT or AMFR knockout C57BL/6 mice as described previously (Nie et al., 2017). Briefly, bone marrow cells were isolated from femurs and tibias and maintained in DMEM (Gibco) with 10 ng/ml recombinant mouse M-CSF for 5–7 d. The human embryonic kidney cell line HEK293T cells and human cervical carcinoma HeLa cell line from ATCC were cultured in DMEM or RPMI-1640 (Gibco) supplemented with 10% FBS (Gibco) and 1% penicillin/streptomycin (Yeasen Biotech). The human monocytic THP-1 cells from ATCC were maintained in RPMI-1640 and differentiated to macrophages by incubation with 100 ng/ml PMA (Sigma-Aldrich) for 24 h. Human PBMCs were isolated from healthy volunteers through gradient centrifugation using Ficoll-Hypaque (Amersham Bioscience) according to the manufacturer's protocol. All cells were kept in a humidified cell culture incubator at 37°C with 5% CO_2. To isolate pulmonary macrophages, mice lungs were perfused with sterile PBS, after which lung lobes were excised and digested using collagenase D (1.0 mg/ml) and DNase I (50 U/ml) as previously described (Nie et al., 2017). Cells were left to adhere for 1 h in serum-free medium, and non-adherent cells (such as lymphocytes) were washed away. Macrophages were lysed in radioimmunoprecipitation assay buffer for protein analysis or in TRIzol for mRNA detection.

Animal models

For the OVA-induced asthma model, female mice (6–8 wk) were sensitized by an i.p. injection of 75 µg OVA emulsified in 2 mg of Imject Alum adjuvant in a total volume of 200 µl on days 0 and 10. On days 21, 22, and 23, mice were challenged with OVA (50 µg in 40 µl PBS) i.t. under pentobarbital sodium anesthesia. Mice were sacrificed on day 25, and peripheral blood, BALF, and lung tissues were collected for further studies. In certain experiments, we administered GM-CSF i.t. (0.4 µg, together with 75 µg OVA in 40 µl PBS) to sensitized LysM^{Cre}*Amfr*$^{fl/fl}$ mice (days 21, 22, and 23). For the papain model, female mice (6–8 wk) received 30 µg papain in 40 µl PBS i.t. for three consecutive days and were sacrificed on day 7. For the chitin-induced eosinophil infiltrating model, mice were subjected to i.t. injection of 10 µg chitin alone or combined with 0.4 µg GM-CSF in 40 µl PBS. After 48 h, the mice were euthanized, and samples were collected. At least five mice were in each group of each experiment, and the control mice were treated with sterile PBS without OVA, papain, chitin, or GM-CSF.

AM adoptive transfer

Adoptive transfer of AMs was performed as previously reported (Miki et al., 2021; Qian et al., 2015). For in vivo deletion of

macrophages in lung tissues, mice were sensitized with OVA as described above and treated with 40 µl of clodronate liposome i.t. for two successive days (days 18 and 19). For the AM adoptive transfer study, AMs derived from WT or AMFR knockout mice were then transferred by i.t. injection into the lungs of clodronate liposome-treated and OVA-sensitized WT mice at a density of 5 × 10^5 cells/mouse (40 µl) on day 20. 24 h after AM delivery, the mice were i.t. challenged with OVA for three days (days 21, 22, and 23). On day 25, the mice were sacrificed to analyze allergic asthmatic inflammation (Fig. 3 A).

CIS knockdown in vivo

Similarly, for in vivo knockdown of CIS in mice lung macrophages, OVA-sensitized recipient $LysM^{cre}Amfr^{fl/fl}$ mice with clodronate liposome i.t. treatment received i.t. $Amfr^{-/-}$ BMDMs that were infected with either Scr shRNA or *Cish* shRNA at a density of 5 × 10^5 cells/mouse (40 µl) on day 20. 24 h after macrophage delivery, the mice were i.t. challenged with OVA for 3 d (days 21, 22, and 23). On day 25, the mice were sacrificed to analyze allergic asthmatic inflammation (Fig. 6 A).

Flow cytometry assay and cell sorting

Cells were incubated with Fc blocking anti-mouse CD16/32 antibody (BD Bioscience) before staining. Cells were incubated with the flow antibodies for 45 min at 4°C for surface staining. For intracellular staining, cells were stimulated with the Cell Activation Cocktail (423304; BioLegend) for 6 h before blocking. Cells were surface stained, fixed, and permeabilized using commercial kits (420801 and 421002; BioLegend), as well as stained using anti-human or anti-mouse GM-CSF Ab. All samples were subjected to flow cytometry (LSRFortessa TM X-20; BD Bioscience), and data were analyzed using FlowJo software. For AM sorting, cells were obtained from the BALF and stained with anti-mouse CD11c and anti-mouse Siglec-F Abs. The AMs (high CD11c and Siglec-F expression) were then sorted through the flow cytometer (BD & FACS Aria III). To sort cells from lung tissues, lungs were perfused with sterile PBS, after which lung lobes were excised and digested using collagenase D (1.0 mg/ml) and DNase I (50 U/ml) through Miltenyi Biotec gentleMACS Octo Dissociator with Heaters, following the 37C-m-LDK-1 program (Miltenyi Biotec). Digested lung tissues were passed through 40-µm cell strainers to obtain a single-cell suspension. After lysis of RBCs, cells were stained with indicated combinations of antibodies and sorted as previously described. Dead cells were excluded by staining with Zombie UV Fixable Viability Kit (423108; BioLegend). Each cell lineage was identified as follows: AMs, $CD45^+CD64^+$ $F4/80^+CD11c^+Siglec\text{-}F^+CD11b^-$; IMs, $CD45^+CD64^+$ $F4/80^+CD11c^-Siglec\text{-}F^-CD11b^+$; monocytes (Mono), $CD45^+CD64^{\pm}CD11b^+$ $F4/80^{low}$; neutrophils (Neu), $CD45^+CD64^-Ly6G^+CD11b^+$; eosinophils (Eos), $CD45^+CD64^-CD11c^-Siglec\text{-}F^+$; and DCs, $CD45^+CD64^-Siglec\text{-}F^-MHC\ II^+$.

RNA isolation and sequencing

Total RNA was isolated using TRIzol reagent according to the manufacturer's instructions. RNA integrity was evaluated using an Agilent 2100 Bioanalyzer (Agilent Technologies). The libraries were established using TruSeq Stranded mRNA LT Sample Prep Kit (Illumina). RNA-seq and analysis were performed by OE Biotech Co.

Immunoprecipitation and Western blot analysis

Assays were conducted as previously reported (Liang et al., 2020). Cells were lysed in radioimmunoprecipitation assay buffer (Beyotime Biotechnology) supplemented with a protease inhibitor cocktail (Sigma-Aldrich). Cell lysates were then centrifuged at 4°C, and the supernatants were collected as extracted protein. These extracts were incubated with the Protein G Agarose beads (Millipore) for 1 h to remove nonspecific binding protein. Afterward, protein extracts were incubated overnight with protein A/G agarose beads along with the antibody, in constant rotation at 4°C. The immune complex was then washed and subjected to immunoblot analysis. For Western blot, proteins were transferred to a nitrocellulose membrane (GE Healthcare Bio-Science). After incubation with primary and secondary antibodies, chemiluminescence of blots was developed using an ECL detection kit (Thermo Fisher Scientific) and detected by the ChemiDoc XRS+ from Bio-Rad. Band intensity was quantified by a densitometric analysis using ImageJ software (National Institutes of Health).

Immunofluorescence staining

Cells were fixed in 4% buffered paraformaldehyde and permeabilized in 0.1% Triton X-100 (Sigma-Aldrich). Subsequently, cells were blocked with 1% BSA (Sigma-Aldrich) and incubated with primary antibodies overnight at 4°C, after which the secondary antibodies (Alexa Flour 488–conjugated anti-rabbit and Alexa Flour 594–conjugated anti-mouse) were applied. The cell nuclei and ER were stained with DAPI and ER-tracker, respectively. Images were captured (63× objective) using the Leica Microsystems CMS GmbH Am Friedensplatz confocal laser scanning microscope (TSC SP8; Leica).

Plasmid construction

The cDNA of AMFR, CIS, SOCS1, SOCS2, SOCS3, STAT5a/b, TSLPR, and IL-7R were obtained using standard PCR techniques from BMDMs or mouse lung tissues and inserted into pcDNA3.1-Flag, pcDNA3.1-Myc, or pcDNA3.1-HA eukaryotic expression vectors as reported previously (Zhu et al., 2017). Plasmid encoding Ub was a gift from Prof. Baoxue Ge (Shanghai Tongji University, China). Truncated mutant vectors AMFR ΔRING finger motif, AMFR ΔCUE domain, AMFR p97/ΔVCP-interacting motif, CIS ΔSH2 domain, CIS ΔSOCS box, CIS-K59R, CIS-K72R, CIS-K98R, CIS-K121R, CIS-K188R, CIS-K208R, Ub-K6, Ub-K11, Ub-K27, Ub-K29, Ub-K33, Ub-K48, Ub-K63, and Ub-K48R were constructed using the KOD-Plus-Mutagenesis Kit (SMK-101; Toyobo) following manufacturer's instructions. The cDNA encoding Myc-tagged CIS (WT and K98R) was subcloned into the lentivirus plasmid pGMLV-CMV-PGK-Puro (Genomeditech). Plasmids encoding all plasmid DNAs for transfection were extracted with Favorprep plasmid Extraction Mini kits (Favorgen). All constructs were confirmed by sequencing.

Lentiviral constructs and transduction

The lentiviruses carrying shRNA targeting AMFR or CIS were purchased from Genomeditech. The shRNA sequences used are

shown in Table S6. The recombinant lentiviruses were amplified, purified, and stored as described. For lentivirus transduction, BMDMs, THP-1 cells, or PBMCs were incubated with lentiviral supernatants and polybrene (TR1003; Sigma-Aldrich). After 48 h, cells were lysed to confirm knockdown efficiency. In addition, transfected cells were stimulated with different treatments for further experiments.

qRT-PCR

Total RNA was isolated from tissues or cells using TRIzol reagent (Invitrogen) and was reverse transcribed to cDNA using ReverTra Ace qPCR RT kit (Toyobo) as reported (Wu et al., 2018). Gene-specific qRT-PCR was performed using primers and probes from SYBR Green Real-time PCR Master Mix with the StepOne Plus system (Thermo Fisher Scientific). The results were normalized against GAPDH expression. The primer sequences are shown in Table S5. The ΔΔCt method was used to calculate mRNA levels compared with the control group.

ELISA

The concentrations of IL-4 (M4000B), IL-5 (M5000), and IL-13 (M1300CB) in BALF were measured by ELISA, according to the manufacturer's protocols (R&D Systems). Total IgE was measured in serum samples using a mouse uncoated ELISA Kit (88-50460-86; eBioscience), in accordance with the manufacturer's instructions.

Histopathology assay

Lung tissues were fixed in 4% paraformaldehyde, embedded in paraffin, excised into 5-µm sections, and placed on adhesion microscope slides. After being deparaffinized and dehydrated, sections were stained using H&E and PAS to assess cell infiltration and mucus production. For immunofluorescence and immunohistochemical analyses, the paraffin-embedded lung sections were deparaffinized using dimethylbenzene. Antigen retrieval was achieved using EDTA, after which sections were incubated with anti-AMFR and anti-CD68 antibodies (both 1:100) at 4°C overnight. Images were captured using the Pannoramic Scanner (Pannoramic DESK, P-MIDI, P250, P1000; 3D HISTECH; Hungary).

Statistical analysis

Data are presented as mean ± SD ($n \geq 3$). One- or two-way ANOVA or Student's t test was performed for multiple comparisons as necessary. The criterion of statistical significance was $P < 0.05$, and symbols indicate P values as follows: *, $P < 0.05$; **, $P < 0.01$; ***, $P < 0.001$; ****, $P < 0.0001$. Statistical analyses of the data were conducted with GraphPad Prism 5 software.

Online supplemental material

Fig. S1 shows sorting strategy of AMs, IMs, monocytes, neutrophils, eosinophils, and DCs and GO enrichment analysis of DEGs in OVA- and papain-induced models. Fig. S2 shows generation and identification of myeloid-specific AMFR-deficient ($LysM^{Cre}Amfr^{fl/fl}$) mice. Fig. S3 shows that AMFR is required for TSLP signaling. Fig. S4 shows that supplementing with GM-CSF restores chitin-induced eosinophil migration in $LysM^{Cre}Amfr^{fl/fl}$ mice. Fig. S5 shows that AMFR promotes the degradation of CIS through proteasome pathway. Table S1 shows DEGs in the OVA vs. PBS group. Table S2 shows DEGs in the papain vs. PBS group. Table S3 shows 205 E3 Ub ligases genes in the GO database. Table S4 shows primers and probes used for identification of myeloid-specific AMFR-deficient ($LysM^{Cre}Amfr^{fl/fl}$) mice. Table S5 shows primers and probes used for qRT-PCR. Table S6 shows primers and probes used for RNAi.

Data availability

The RNA-seq data have been deposited in the National Center for Biotechnology Information Sequence Read Archive database under the accession code SRP332634. Other data that support the findings of this study are available within the article and its supplemental tables and figures.

Acknowledgments

This work was supported by grants from the National Natural Science Foundation of China (81973329, 82073858, 82173821, 81773741), Natural Science Foundation of Shanghai (21ZR1432700), and Shanghai Jiao Tong University Scientific and Technological Innovation Funds (19X160010005).

Author contributions: L. Sun and F. Qian conceived the study. H. Zhang, R. Wei, X. Yang, L. Xu, H. Jiang, M. Li, H. Zhang, and Z. Chen designed, performed, and interpreted experimental data. H. Jiang supported FACS analysis. L. Sun, F. Qian, and H. Zhang wrote the paper. All authors read and approved the final manuscript.

Disclosures: The authors declare no competing financial interests.

Submitted: 27 August 2021
Revised: 2 January 2022
Accepted: 2 February 2022

References

Adhikary, P.P., Z. Tan, B.D.G. Page, and S. Hedtrich. 2021. TSLP as druggable target: A silver-lining for atopic diseases? *Pharmacol. Ther.* 217:107648. https://doi.org/10.1016/j.pharmthera.2020.107648

Al-Shami, A., R. Spolski, J. Kelly, A. Keane-Myers, and W.J. Leonard. 2005. A role for TSLP in the development of inflammation in an asthma model. *J. Exp. Med.* 202:829–839. https://doi.org/10.1084/jem.20050199

Collison, A., L. Hatchwell, N. Verrills, P.A. Wark, A.P. de Siqueira, M. Tooze, H. Carpenter, A.S. Don, J.C. Morris, N. Zimmermann, et al. 2013. The E3 ubiquitin ligase midline 1 promotes allergen and rhinovirus-induced asthma by inhibiting protein phosphatase 2A activity. *Nat. Med.* 19: 232–237. https://doi.org/10.1038/nm.3049

Corren, J., J.R. Parnes, L. Wang, M. Mo, S.L. Roseti, J.M. Griffiths, and R. van der Merwe. 2017. Tezepelumab in adults with uncontrolled asthma. *N. Engl. J. Med.* 377:936–946. https://doi.org/10.1056/NEJMoa1704064

Delconte, R.B., T.B. Kolesnik, L.F. Dagley, J. Rautela, W. Shi, E.M. Putz, K. Stannard, J.G. Zhang, C. Teh, M. Firth, et al. 2016. CIS is a potent checkpoint in NK cell-mediated tumor immunity. *Nat. Immunol.* 17: 816–824. https://doi.org/10.1038/ni.3470

Evren, E., E. Ringqvist, and T. Willinger. 2020. Origin and ontogeny of lung macrophages: From mice to humans. *Immunology*. 160:126–138. https://doi.org/10.1111/imm.13154

Fahy, J.V. 2015. Type 2 inflammation in asthma–present in most, absent in many. *Nat. Rev. Immunol.* 15:57–65. https://doi.org/10.1038/nri3786

Fairbank, M., P. St-Pierre, and I.R. Nabi. 2009. The complex biology of autocrine motility factor/phosphoglucose isomerase (AMF/PGI) and its receptor, the gp78/AMFR E3 ubiquitin ligase. *Mol. Biosyst.* 5:793–801. https://doi.org/10.1039/b820820b

Fang, S., M. Ferrone, C. Yang, J.P. Jensen, S. Tiwari, and A.M. Weissman. 2001. The tumor autocrine motility factor receptor, gp78, is a ubiquitin protein ligase implicated in degradation from the endoplasmic reticulum. *Proc. Natl. Acad. Sci. USA*. 98:14422–14427. https://doi.org/10.1073/pnas.251401598

Fehervari, Z. 2015. Alveolar macrophages in asthma. *Nat. Immunol.* 16:64. https://doi.org/10.1038/ni.3065

Fu, M., P. St-Pierre, J. Shankar, P.T. Wang, B. Joshi, and I.R. Nabi. 2013. Regulation of mitophagy by the Gp78 E3 ubiquitin ligase. *Mol. Biol. Cell*. 24:1153–1162. https://doi.org/10.1091/mbc.E12-08-0607

Gschwend, J., S.P.M. Sherman, F. Ridder, X. Feng, H.E. Liang, R.M. Locksley, B. Becher, and C. Schneider. 2021. Alveolar macrophages rely on GM-CSF from alveolar epithelial type 2 cells before and after birth. *J. Exp. Med.* 218:e20210745. https://doi.org/10.1084/jem.20210745

Holgate, S.T. 2012. Innate and adaptive immune responses in asthma. *Nat. Med.* 18:673–683. https://doi.org/10.1038/nm.2731

Hu, H., and S.C. Sun. 2016. Ubiquitin signaling in immune responses. *Cell Res.* 26:457–483. https://doi.org/10.1038/cr.2016.40

Isaksen, D.E., H. Baumann, P.A. Trobridge, A.G. Farr, S.D. Levin, and S.F. Ziegler. 1999. Requirement for stat5 in thymic stromal lymphopoietin-mediated signal transduction. *J. Immunol.* 163:5971–5977

Jiang, X., and Z.J. Chen. 2011. The role of ubiquitylation in immune defence and pathogen evasion. *Nat. Rev. Immunol.* 12:35–48. https://doi.org/10.1038/nri3111

Joshi, N., J.M. Walter, and A.V. Misharin. 2018. Alveolar macrophages. *Cell Immunol.* 330:86–90. https://doi.org/10.1016/j.cellimm.2018.01.005

Joshi, V., A. Upadhyay, A. Kumar, and A. Mishra. 2017. Gp78 E3 ubiquitin ligase: Essential functions and contributions in proteostasis. *Front Cell Neurosci.* 11:259. https://doi.org/10.3389/fncel.2017.00259

Kabata, H., K. Moro, S. Koyasu, and K. Asano. 2015. Group 2 innate lymphoid cells and asthma. *Allergol. Int.* 64:227–234. https://doi.org/10.1016/j.alit.2015.03.004

Kishta, O.A., A. Sabourin, L. Simon, T. McGovern, M. Raymond, T. Galbas, A. Majdoubi, S. Ishido, J.G. Martin, and J. Thibodeau. 2018. March1 E3 ubiquitin ligase modulates features of allergic asthma in an ovalbumin-induced mouse model of lung inflammation. *J. Immunol. Res.* 2018: 3823910. https://doi.org/10.1155/2018/3823910

Kulikauskaite, J., and A. Wack. 2020. Teaching old dogs new tricks? The plasticity of lung alveolar macrophage subsets. *Trends Immunol.* 41: 864–877. https://doi.org/10.1016/j.it.2020.08.008

Lai, J.F., L.J. Thompson, and S.F. Ziegler. 2020. TSLP drives acute T_H2-cell differentiation in lungs. *J. Allergy Clin. Immunol.* 146:1406–1418.e7. https://doi.org/10.1016/j.jaci.2020.03.032

Lambrecht, B.N., H. Hammad, and J.V. Fahy. 2019. The cytokines of asthma. *Immunity*. 50:975–991. https://doi.org/10.1016/j.immuni.2019.03.018

Li, H.B., J. Tong, S. Zhu, P.J. Batista, E.E. Duffy, J. Zhao, W. Bailis, G. Cao, L. Kroehling, Y. Chen, et al. 2017. m(6)A mRNA methylation controls T cell homeostasis by targeting the IL-7/STAT5/SOCS pathways. *Nature*. 548: 338–342. https://doi.org/10.1038/nature23450

Liang, Q., W. Cai, Y. Zhao, H. Xu, H. Tang, D. Chen, F. Qian, and L. Sun. 2020. Lycorine ameliorates bleomycin-induced pulmonary fibrosis via inhibiting NLRP3 inflammasome activation and pyroptosis. *Pharmacol. Res.* 158:104884. https://doi.org/10.1016/j.phrs.2020.104884

Lin, S.C., H.W. Lin, and B.L. Chiang. 2017. Association of croup with asthma in children: A cohort study. *Medicine (Baltimore)*. 96:e7667. https://doi.org/10.1097/md.0000000000007667

Liu, S.S., C. Liu, X.X. Lv, B. Cui, J. Yan, Y.X. Li, K. Li, F. Hua, X.W. Zhang, J.J. Yu, et al. 2021. The chemokine CCL1 triggers an AMFR-SPRY1 pathway that promotes differentiation of lung fibroblasts into myofibroblasts and drives pulmonary fibrosis. *Immunity*. 54:2433–2435.e2048. https://doi.org/10.1016/j.immuni.2021.06.008

Liu, X., Q. Wang, W. Chen, and C. Wang. 2013. Dynamic regulation of innate immunity by ubiquitin and ubiquitin-like proteins. *Cytokine Growth Factor Rev.* 24:559–570. https://doi.org/10.1016/j.cytogfr.2013.07.002

Liu, Y.C. 2007. The E3 ubiquitin ligase Itch in T cell activation, differentiation, and tolerance. *Semin. Immunol.* 19:197–205. https://doi.org/10.1016/j.smim.2007.02.003

Luo, Y., J.M. Long, C. Lu, S.L. Chan, E.L. Spangler, P. Mascarucci, A. Raz, D.L. Longo, M.P. Mattson, D.K. Ingram, and NP Weng. 2002. A link between maze learning and hippocampal expression of neuroleukin and its receptor gp78. *J. Neurochem.* 80:354–361. https://doi.org/10.1046/j.0022-3042.2001.00707.x

Miki, H., H. Pei, D.T. Gracias, J. Linden, and M. Croft. 2021. Clearance of apoptotic cells by lung alveolar macrophages prevents development of house dust mite-induced asthmatic lung inflammation. *J. Allergy Clin. Immunol.* 147:1087–1092.e3. https://doi.org/10.1016/j.jaci.2020.10.005

Moore, W.C., A.M. Fitzpatrick, X. Li, A.T. Hastie, H. Li, D.A. Meyers, and E.R. Bleecker. 2013. Clinical heterogeneity in the severe asthma research program. *Ann. Am. Thorac. Soc.* 10:S118–S124. https://doi.org/10.1513/AnnalsATS.201309-307AW

Nie, Y., L. Sun, Y. Wu, Y. Yang, J. Wang, H. He, Y. Hu, Y. Chang, Q. Liang, J. Zhu, et al. 2017. AKT2 regulates pulmonary inflammation and fibrosis via modulating macrophage activation. *J. Immunol.* 198:4470–4480. https://doi.org/10.4049/jimmunol.1601503

Nobs, S.P., M. Kayhan, and M. Kopf. 2019. GM-CSF intrinsically controls eosinophil accumulation in the setting of allergic airway inflammation. *J. Allergy Clin. Immunol.* 143:1513–1524.e1512. https://doi.org/10.1016/j.jaci.2018.08.044

Nobs, S.P., L. Pohlmeier, F. Li, M. Kayhan, B. Becher, and M. Kopf. 2021. GM-CSF instigates a dendritic cell-T-cell inflammatory circuit that drives chronic asthma development. *J. Allergy Clin. Immunol.* 147: 2118–2133.e2113. https://doi.org/10.1016/j.jaci.2020.12.638

Palmer, D.C., and N.P. Restifo. 2009. Suppressors of cytokine signaling (SOCS) in T cell differentiation, maturation, and function. *Trends Immunol.* 30:592–602. https://doi.org/10.1016/j.it.2009.09.009

Peltola, K.J., K. Paukku, T.L. Aho, M. Ruuska, O. Silvennoinen, and P.J. Koskinen. 2004. Pim-1 kinase inhibits STAT5-dependent transcription via its interactions with SOCS1 and SOCS3. *Blood*. 103:3744–3750. https://doi.org/10.1182/blood-2003-09-3126

Popovic, D., D. Vucic, and I. Dikic. 2014. Ubiquitination in disease pathogenesis and treatment. *Nat. Med.* 20:1242–1253. https://doi.org/10.1038/nm.3739

Puttur, F., L.G. Gregory, and C.M. Lloyd. 2019. Airway macrophages as the guardians of tissue repair in the lung. *Immunol. Cell Biol.* 97:246–257. https://doi.org/10.1111/imcb.12235

Qian, F., J. Deng, Y.G. Lee, J. Zhu, M. Karpurapu, S. Chung, J.N. Zheng, L. Xiao, G.Y. Park, and J.W. Christman. 2015. The transcription factor PU.1 promotes alternative macrophage polarization and asthmatic airway inflammation. *J. Mol. Cell Biol.* 7:557–567. https://doi.org/10.1093/jmcb/mjv042

Qiao, G., H. Ying, Y. Zhao, Y. Liang, H. Guo, H. Shen, Z. Li, J. Solway, E. Tao, Y.J. Chiang, et al. 2014. E3 ubiquitin ligase Cbl-b suppresses proallergic T cell development and allergic airway inflammation. *Cell Rep.* 6: 709–723. https://doi.org/10.1016/j.celrep.2014.01.012

Reese, T.A., H.E. Liang, A.M. Tager, A.D. Luster, N. Van Rooijen, D. Voehringer, and R.M. Locksley. 2007. Chitin induces accumulation in tissue of innate immune cells associated with allergy. *Nature*. 447:92–96. https://doi.org/10.1038/nature05746

Sahoo, A. 2014. E3 ligases in T helper 2-mediated pathogenesis. *Immunome Res.* 11. https://doi.org/10.4172/1745-7580.1000086

Sahoo, A., A. Alekseev, L. Obertas, and R. Nurieva. 2014. Grail controls Th2 cell development by targeting STAT6 for degradation. *Nat. Commun.* 5: 4732. https://doi.org/10.1038/ncomms5732

Schuijs, M.J., M.A. Willart, K. Vergote, D. Gras, K. Deswarte, M.J. Ege, F.B. Madeira, R. Beyaert, G. van Loo, F. Bracher, et al. 2015. Farm dust and endotoxin protect against allergy through A20 induction in lung epithelial cells. *Science*. 349:1106–1110. https://doi.org/10.1126/science.aac6623

Song, Y., Y. Wu, X. Li, Y. Shen, Y. Ding, H. Zhu, F. Liu, K. Yu, L. Sun, and F. Qian. 2018. Protostemonine attenuates alternatively activated macrophage and DRA-induced asthmatic inflammation. *Biochem. Pharmacol.* 155:198–206. https://doi.org/10.1016/j.bcp.2018.07.003

Stern, J., J. Pier, and A.A. Litonjua. 2020. Asthma epidemiology and risk factors. *Semin. Immunopathol.* 42:5–15. https://doi.org/10.1007/s00281-020-00785-1

Walker, J.A., and A.N.J. McKenzie. 2018. T(H)2 cell development and function. *Nat. Rev. Immunol.* 18:121–133. https://doi.org/10.1038/nri.2017.118

Wang, Q., X. Liu, Y. Cui, Y. Tang, W. Chen, S. Li, H. Yu, Y. Pan, and C. Wang. 2014. The E3 ubiquitin ligase AMFR and INSIG1 bridge the activation of TBK1 kinase by modifying the adaptor STING. *Immunity*. 41:919–933. https://doi.org/10.1016/j.immuni.2014.11.011

Wu, Y., H. He, Y. Ding, S. Liu, D. Zhang, J. Wang, H. Jiang, D. Zhang, L. Sun, R.D. Ye, and F. Qian. 2018. MK2 mediates macrophage activation and acute lung injury by regulating let-7e miRNA. *Am. J. Physiol. Lung Cell Mol. Physiol.* 315:L371–l381. https://doi.org/10.1152/ajplung.00019.2018

Yang, X.O., H. Zhang, B.S. Kim, X. Niu, J. Peng, Y. Chen, R. Kerketta, Y.H. Lee, S.H. Chang, D.B. Corry, et al. 2013. The signaling suppressor CIS controls proallergic T cell development and allergic airway inflammation. *Nat. Immunol.* 14:732–740. https://doi.org/10.1038/ni.2633

Ying, Z., H. Wang, H. Fan, and G. Wang. 2011. The endoplasmic reticulum (ER)-associated degradation system regulates aggregation and degradation of mutant neuroserpin. *J. Biol. Chem.* 286:20835–20844. https://doi.org/10.1074/jbc.M110.200808

Zhu, Z., L. Sun, R. Hao, H. Jiang, F. Qian, and R.D. Ye. 2017. Nedd8 modification of Cullin-5 regulates lipopolysaccharide-induced acute lung injury. *Am. J. Physiol. Lung Cell Mol. Physiol.* 313:L104–l114. https://doi.org/10.1152/ajplung.00410.2016

Supplemental material

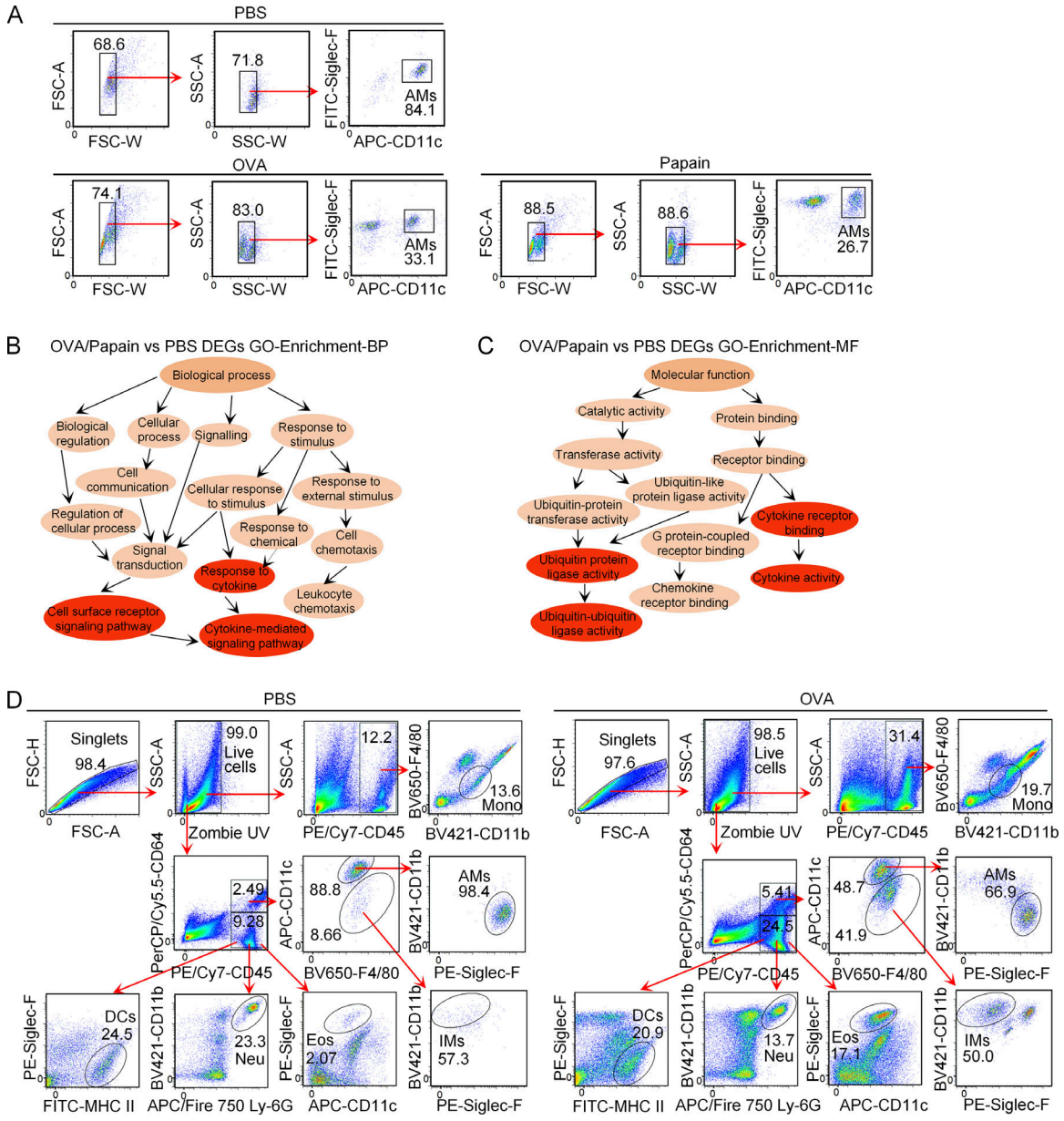

Figure S1. **Sorting strategy of AMs, IMs, monocytes, neutrophils, eosinophils, and DCs and GO enrichment analysis of DEGs in OVA- and papain-induced models. (A)** AMs ($CD11c^+Siglec\text{-}F^+$) from OVA- or papain-induced mice BALF were sorted using flow cytometry and subjected to RNA-seq. FSC, forward scatter; SSC, side scatter. **(B and C)** GO enrichment analysis of biological process (BP) and molecular function (MF) from the RNA-seq data of OVA- and papain-induced asthmatic AMs, compared with AMs from the PBS group. **(D)** AMs ($CD45^+CD64^+F4/80^+CD11c^+Siglec\text{-}F^+CD11b^-$), IMs ($CD45^+CD64^+F4/80^+CD11c^-Siglec\text{-}F^-CD11b^+$), monocytes (Mono, $CD45^+CD64^{\pm}CD11b^+F4/80^{low}$), neutrophils (Neu, $CD45^+CD64^-Ly6G^+CD11b^+$), eosinophils (Eos, $CD45^+CD64^-CD11c^-Siglec\text{-}F^+$), and DCs ($CD45^+CD64^-Siglec\text{-}F^-MHC\ II^+$) from PBS and OVA mice lung tissues were sorted using flow cytometry and subjected to qRT-PCR analysis. Numbers in flow plots indicate percentages. Data shown are representative of three independent experiments (n = 3, A–D).

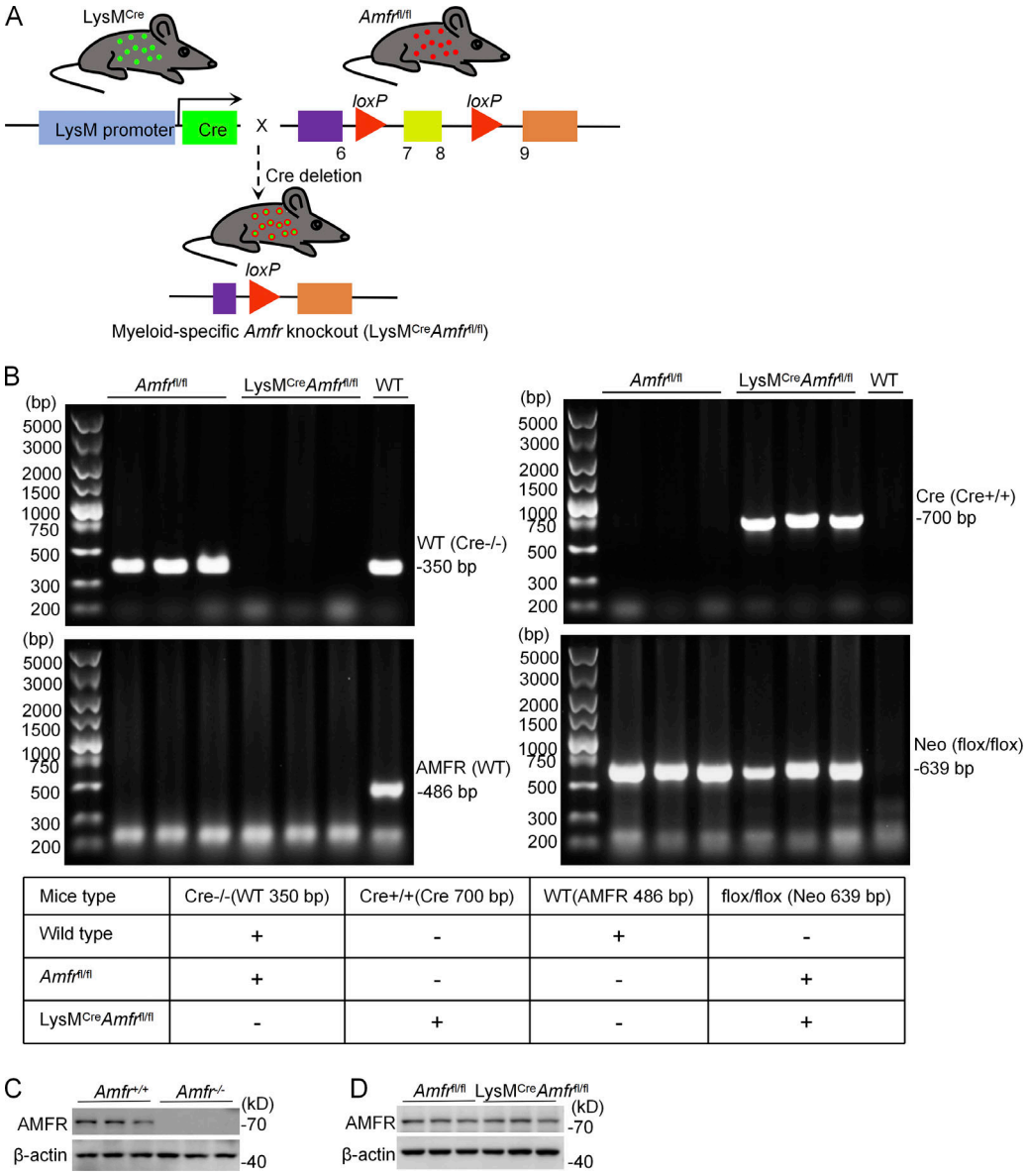

Mice type	Cre-/-(WT 350 bp)	Cre+/+(Cre 700 bp)	WT(AMFR 486 bp)	flox/flox (Neo 639 bp)
Wild type	+	-	+	-
Amfr$^{fl/fl}$	+	-	-	+
LysM^{Cre}*Amfr*$^{fl/fl}$	-	+	-	+

Figure S2. **Generation and identification of myeloid-specific AMFR-deficient (LysM^{Cre}*Amfr*$^{fl/fl}$) mice. (A)** Mice conditionally containing a loxP sequence flanking the seventh and eighth exon of *Amfr* gene (*Amfr*$^{fl/fl}$) were crossed with Lysozyme M-Cre mice, which expressed Cre recombinase downstream of the lysozyme LysM promoter (LysM^{Cre}). **(B)** Mice were genotyped using PCR analysis of DNA obtained from tail snip. AMFR-deficient (LysM^{Cre}*Amfr*$^{fl/fl}$) mice have a 639-bp product for the loxP-targeted allele and a 700-bp product for the LysM-Cre allele. *Amfr*$^{fl/fl}$ mice have a 639-bp product for the loxP-targeted allele and a 350-bp product for the WT allele. **(C)** Protein expression of AMFR in BMDMs. **(D)** Protein expression of AMFR in lung tissues. All genotypes were generated on a pure C57BL/6 background. Data are presented from one representative of three independent experiments (n = 3, B–D). Source data are available for this figure: SourceData FS2.

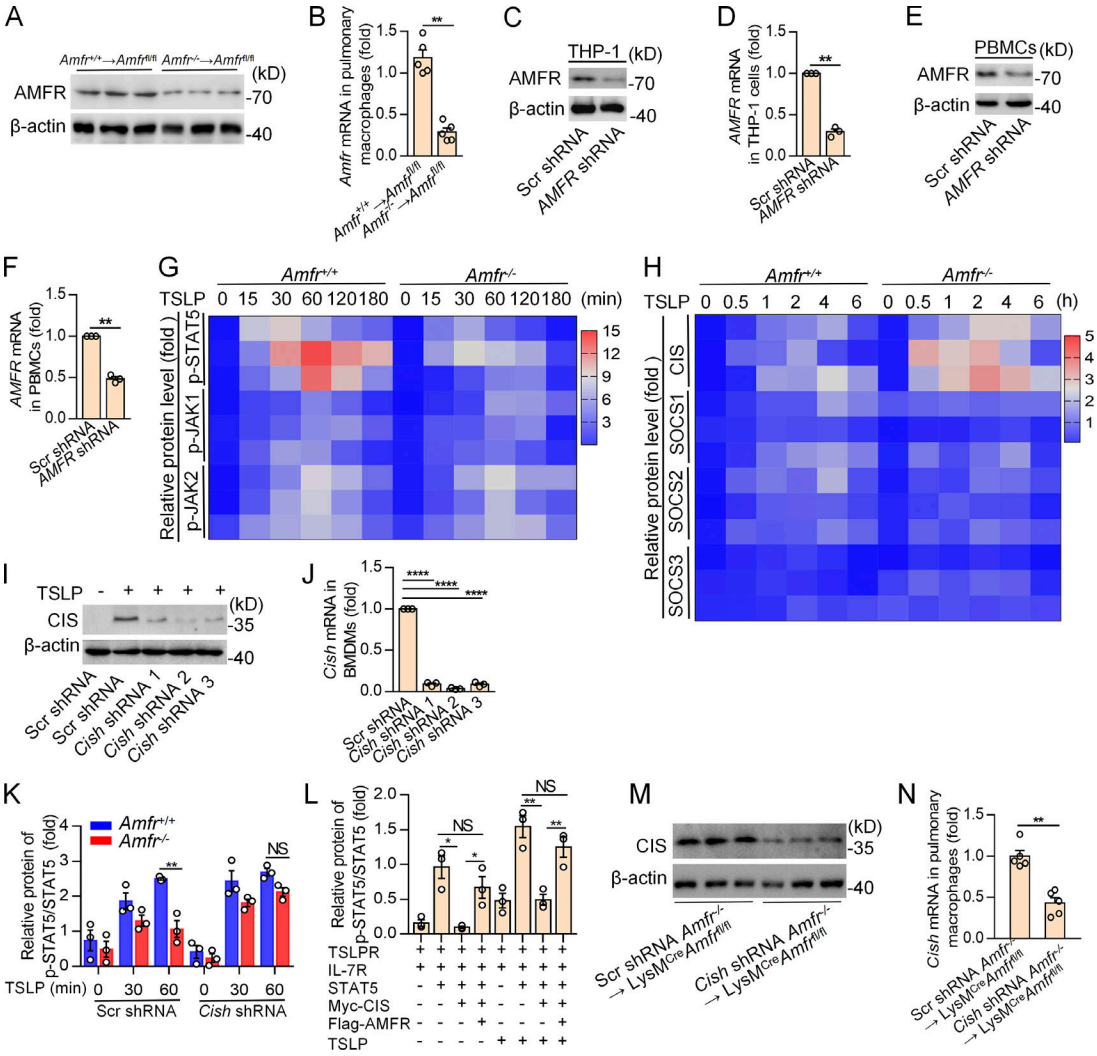

Figure S3. **AMFR is required for TSLP signaling. (A and B)** The protein and mRNA expression of AMFR in pulmonary macrophages after AM adoptive transfer. **(C–F)** The knockdown efficiency of *AMFR* shRNA in THP-1 cells and PBMCs was detected using Western blot (C and E) and qRT-PCR analysis (D and F). **(G and H)** Immunoblot analysis of phosphorylated (p-) STAT5, JAK1, JAK2, total STAT5, JAK1, JAK2, CIS, SOCS1, SOCS2, SOCS3, and β-actin in whole-cell lysates of BMDMs stimulated with TSLP (10 ng/ml) at various time points. The quantification of the blots was performed using ImageJ and is shown in a heatmap. **(I and J)** The knockdown efficiency of *Cish* shRNAs in BMDMs was detected using Western blot (I) and qRT-PCR analysis (J). **(K)** Immunoblot analysis of phosphorylated and total STAT5 protein levels in BMDMs transfected with lentivirus-mediated *Cish* shRNA or Scr shRNA, and 48 h later, stimulated with TSLP (10 ng/ml) at various time points. **(L)** Immunoblot analysis of phosphorylated and total STAT5 in HEK293T cells transfected with plasmids encoding IL-7R, TSLPR, STAT5, Flag-AMFR, and Myc-CIS, and 48 h later, stimulated with TSLP (10 ng/ml) for 60 min. The quantification of the blots was performed using ImageJ. **(M and N)** The knockdown efficiency of CIS in vivo was detected using Western blot (M) and qRT-PCR analysis (N). Data shown are representative of three independent experiments (A, C, E, I, and M). Each symbol represents one mouse, and data are presented as mean ± SD from one representative of three independent experiments (n = 5 mice per group per experiment; B and N). Each symbol represents data from an independent experiment, and data are presented as mean ± SD from one representative of three independent experiments (n = 3; D, F, and J–L). *, P < 0.05; **, P < 0.01; ****, P < 0.0001 (Student's t test, B, D, F, J, and N; two-way ANOVA with Tukey's post hoc analysis, K; and one-way ANOVA with Tukey's post hoc analysis, L). Source data are available for this figure: SourceData FS3.

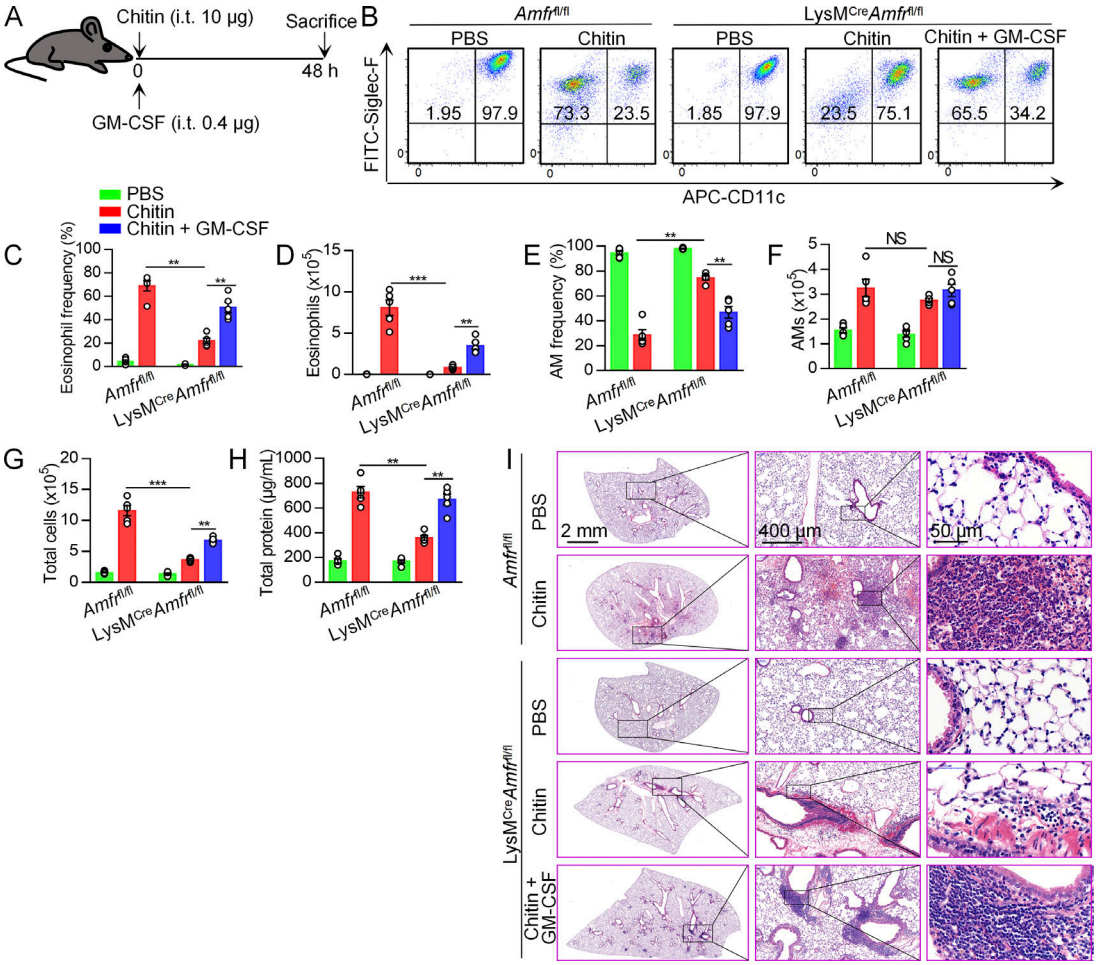

Figure S4. **Supplementing with GM-CSF restores chitin-induced eosinophil migration in LysM^{Cre}*Amfr*$^{fl/fl}$ mice. (A)** Schematic graph of the chitin-induced eosinophil migration model supplementing with exogenous GM-CSF. **(B)** Mice were treated as in A. BALF cells were stained with APC-CD11c and FITC-Siglec-F. Eosinophils (Eos, CD11c$^-$Siglec-F$^+$) and AMs (AMs, CD11c$^+$Siglec-F$^+$) were identified. **(C and D)** Eosinophil percentage and number in BALF. **(E and F)** AM percentage and number in BALF. **(G and H)** Total cell number and total protein concentration in BALF. **(I)** Representative histopathology of lung tissues stained with H&E. Scale bars: 2 mm, 400 μm, and 50 μm. Numbers in flow plots indicate percentages. Data shown are representative of three independent experiments (B and I). Each symbol represents an individual mouse, and data are presented as mean ± SD from one representative of three independent experiments (n = 5 mice per group per experiment; C–H). **, P < 0.01; ***, P < 0.001 (two-way ANOVA with Tukey's post hoc analysis, C–H).

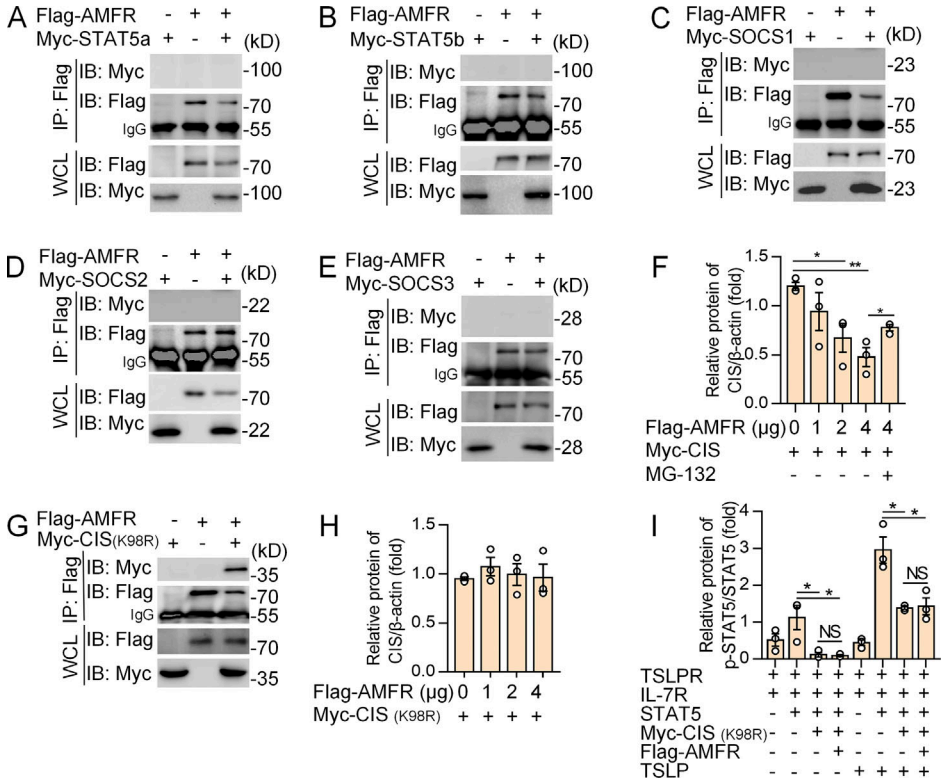

Figure S5. **AMFR promotes the degradation of CIS through proteasome pathway. (A–E)** Coimmunoprecipitation and immunoblot analysis of HEK293T cells cotransfected with Flag-AMFR and Myc-STAT5a (A), Myc-STAT5b (B), Myc-SOCS1 (C), Myc-SOCS2 (D), and Myc-SOCS3 (E), followed by IP with the anti-Flag Ab. WCL, whole-cell lysate. **(F)** Immunoblot analysis of CIS protein levels in HEK293T cells transfected with Myc-CIS with different amounts of Flag-AMFR. The proteasome inhibitor MG132 was added to treat the cells for 4 h, if necessary. β-Actin acted as a loading control. The quantification of the blots was analyzed by ImageJ. **(G)** Coimmunoprecipitation and immunoblot analysis of HEK293T cells cotransfected with Flag-AMFR and Myc-CIS (K98R), followed by immunoprecipitation with the anti-Flag Ab. **(H)** Immunoblot analysis of CIS protein levels in HEK293T cells transfected with Myc-CIS (K98R) with different amounts of Flag-AMFR. β-Actin acted as a loading control. The quantification of the blots was performed using ImageJ. **(I)** Immunoblot analysis of phosphorylated and total STAT5 in HEK293T cells transfected with plasmids encoding IL-7R, TSLPR, STAT5, Flag-AMFR, and Myc-CIS (K98R), and after 48 h, stimulated with TSLP (10 ng/ml) for 60 min. The quantification of the blots was performed using ImageJ. Data are presented from one representative of three independent experiments (n = 3, A–E, and G), or are presented as mean ± SD from three independent experiments with biological duplicates in each (F, H, and I). *, P < 0.05; **, P < 0.01 (one-way ANOVA with Dunn's post hoc analysis, F, H, and I). Source data are available for this figure: SourceData FS5.

Provided online are Table S1, Table S2, Table S3, Table S4, Table S5, and Table S6. Table S1 shows DEGs in the OVA vs. PBS group. Table S2 shows DEGs in the papain vs. PBS group. Table S3 shows 205 E3 Ub ligases genes in the GO database. Table S4 shows primers and probes used for identification of myeloid-specific AMFR-deficient (LysM^{Cre}*Amfr*$^{fl/fl}$) mice. Table S5 shows primers and probes used for qRT-PCR. Table S6 shows primers and probes used for RNAi.